Journal of Computational Physics 307 (2016) 355–377

Contents lists available at ScienceDirect

Journal of Computational Physics

www.elsevier.com/locate/jcp

# Topology optimization in thermal-fluid flow using the lattice Boltzmann method

Kentaro Yaji [a,*], Takayuki Yamada [a], Masato Yoshino [b], Toshiro Matsumoto [c], Kazuhiro Izui [a], Shinji Nishiwaki [a]

[a] Department of Mechanical Engineering and Science, Graduate School of Engineering, Kyoto University, Kyoto 615-8540, Japan
[b] Institute of Engineering, Academic Assembly, Shinshu University, Nagano 380-8553, Japan
[c] Department of Mechanical Engineering and Science, Graduate School of Engineering, Nagoya University, Aichi 464-8603, Japan

ARTICLE INFO

*Article history:*
Received 20 May 2015
Received in revised form 6 November 2015
Accepted 2 December 2015
Available online 11 December 2015

*Keywords:*
Topology optimization
Adjoint lattice Boltzmann method
Discrete velocity Boltzmann equation
Thermal-fluid flow

ABSTRACT

This paper proposes a topology optimization method for thermal-fluid flow problems using the lattice Boltzmann method (LBM). The design sensitivities are derived based on the adjoint lattice Boltzmann method (ALBM), whose basic idea is that the adjoint problem is first formulated using a continuous adjoint approach, and the adjoint problem is then solved using the LBM. In this paper, the discrete velocity Boltzmann equation, in which only the particle velocities are discretized, is introduced to the ALBM to deal with the various boundary conditions in the LBM. The novel sensitivity analysis is applied in two flow channel topology optimization problems: 1) a pressure drop minimization problem, and 2) a heat exchange maximization problem. Several numerical examples are provided to confirm the utility of the proposed method.



## 1. Introduction

The application of structural optimization methods for fluid dynamics problems has been an attractive area of research for engineers and mathematicians. In the field of structural optimization for fluid dynamics problems, the most widely used approach is based on shape optimization, a kind of structural optimization whose main concept is that the geometry of a solid domain can be optimized, to improve performance, by moving the boundary between the fluid and solid domains. In this research field, Pironneau pioneered a shape optimization method for fluid dynamics problems and constructed the basic mathematical theory for obtaining minimum drag body profiles under Stokes flow [1]. The reader is referred to a recent monograph by Mohammadi and Pironneau [2] in which a variety of shape optimization methods are discussed. However, shape optimization methods only allow changes in boundary shapes, so feasible design modifications are limited. This limitation can be overcome by applying topology optimization, which allows the creation of new holes in the design domain during the optimization process, providing enhanced degrees of freedom compared with shape optimization. In fluid flow topology optimization problems, these newly created holes may be either new fluid or solid domains.

Topology optimization in structural mechanics problems is a well-documented field, since Bendsøe and Kikuchi first proposed the so-called homogenization design method [3]. The basic idea of topology optimization is the introduction of an extended design domain, the so-called fixed design domain, and the replacement of the optimization problem with a

* Corresponding author.
*E-mail address:* yaji.kentarou.74v@st.kyoto-u.ac.jp (K. Yaji).

http://dx.doi.org/10.1016/j.jcp.2015.12.008
0021-9991/

material distribution problem, using the characteristic function. The homogenization design method has been applied to a variety of optimization problems, and the density approach, also called the solid isotropic material with penalization (SIMP) method [4], is another currently used topology optimization method. Recent developments in the field of topology optimization have been categorized in a review paper by Sigmund and Maute [5].

Based on the concept of the density approach, Borravall and Petersson [6] pioneered a topology optimization method for minimum power dissipation in Stokes flow problems, where the material distribution in the fixed design domain is represented as either the presence of a fluid or a solid domain. The basic idea of this research is that the fixed design domain is composed of a porous medium governed by the theory of Darcy's law. Thus, the solid and fluid domains in the fixed design domain are represented as porous media of either high or low porosity, and the no-slip boundary condition along the fluid–solid interface can be implicitly satisfied. Based on this methodology, Gersborg-Hansen et al. [7] proposed a topology optimization method for a steady-state fluid flow governed by the Navier–Stokes equations (NSE). Deng et al. [8], and Kreissl et al. [9], extended the steady-state approach to unsteady flow problems. In addition, Evgrafov [10] constructed a mathematical theory to assess the well-posedness of topology optimization problems for the minimization of power dissipation under the incompressible viscous flow.

In most previous research in topology optimization for fluid dynamics problems, the finite element method (FEM) is employed to discretize the flow field governed by the NSE. Although the FEM is a well-studied and accurate approach based on the theory of variational formulation, the computational cost for calculating the flow field dramatically increases when a large-scale computational domain is treated. In particular, due to the inf–sup condition, a high-order shape function must be generally used for the approximation of fluid velocity [11]. Furthermore, an iterative computation, which incurs massive computational cost in large-scale incompressible viscous fluid problems, is necessary to correct the velocity and pressure values so that the conservations of mass and momentum are satisfied.

As an alternative way to solve the flow field, the lattice Boltzmann method (LBM) has become an attractive scheme in the research field of computational fluid dynamics [12–15]. Comparing the coding used in the LBM with that used in conventional schemes such as the finite element and finite volume methods, LBM algorithm is much simpler since the fluid flow is solved using a time evolution equation, the so-called lattice Boltzmann equation (LBE), and the LBM offers a further advantage, its scalability for complex flow problems such as porous, miscible, and immiscible fluid flow problems. In addition, the LBM enables one to avoid the numerical treatment of iterative computation for the correction of fluid velocity and pressure in the incompressible viscous fluid flow. Topology optimization methods that use the LBM are therefore suitable for dealing with large-scale and complex flow optimization problems.

Pingen et al. [16] proposed a topology optimization using the LBM, and obtained optimal configurations similar to those using a conventional approach proposed by Borrvall and Petersson [6]. Based on the study by Pingen et al., Makhija et al. [17] extended this approach to a scalar transport problem using the multi-relaxation time LBM [18] for the maximization problem of mixing efficiency in a mixing device. In addition, Kreissl et al. [19] proposed a topology optimization method using the LBM for a fluid–solid interaction problem for the design of microchannel devices. However, in the above methodologies based on the research of Pingen et al., a large-scale, hence unwieldy, asymmetric matrix is used to solve the adjoint problem during each iteration of the optimization process. Although a specific method for solving this matrix system was later proposed by Pingen et al. [20], this optimization method is not well suited to more complex large-scale flow problems.

To solve identification problems with the LBM, Tekitek et al. [21] proposed a methodology using the adjoint lattice Boltzmann equation (ALBE), and Krause et al. [22,23] recently proposed the so-called adjoint lattice Boltzmann method (ALBM). The basic idea of these approaches is that both the state and adjoint fields are solved using the LBM, which can make use of highly efficient algorithms due to the similarity of the locality properties, and the design sensitivities can therefore be obtained without the use of matrix operations. Due to the different ways in which the adjoint sensitivity analysis is conducted, these approaches can be classified in two categories: 1) methods based on a discrete adjoint approach using the ALBE, in which the sensitivity analysis is conducted using discrete equations and the adjoint equation is therefore derived as a discrete equation, the so-called ALBE, and 2) the ALBM, which is based on a continuous adjoint approach in which the sensitivity analysis is conducted using the continuous Boltzmann equation with the Bhatnagar–Gross–Krook (BGK) approximation [24]. In the latter approach, the adjoint equation is therefore obtained as a continuous equation, whose formulation is similar to that of the Boltzmann equation, which is then discretized using the LBM. Krause et al. [22, 23] investigated the parallel performance of the ALBM and demonstrated that the ALBM is exceptionally useful for obtaining efficient parallel implementations, when compared with already well-established schemes.

In the research field of topology optimization, Yaji et al. [25] proposed a topology optimization method based on the ALBM for solving the pressure drop minimization problem that aims to obtain optimal configurations of the two- and three-dimensional flow channels. On the other hand, Liu et al. [26] successfully applied the ALBE in a topology optimization method for a minimum power dissipation problem. Concerning an additional unique topology optimization approach using the LBM, Yonekura and Kanno [27] recently proposed a topology optimization method for a minimum power dissipation problem in which two computational steps, the gradient optimization algorithm and the LBE, are synchronized so that an optimal configuration is rapidly obtained.

In the ALBM [22,23], the use of the continuous Boltzmann equation prevents the use of the high accuracy boundary conditions that are generally used in the LBM, since the LBM boundary conditions are formulated using discrete particle velocities. Liu et al. [26] recently asserted that most of the boundary conditions for the ALBE had to be defined *a posteriori*, due to the use of a discrete adjoint approach. Although no-slip or periodic boundary conditions naturally influence the adjoint

boundary conditions, their formulation is the same as those of the equations of the state problem, whereas other boundary conditions that are commonly used in fluid flow analysis, such as prescribed velocity or pressure boundary conditions (e.g., [28]), obviously require different formulations than those of the adjoint boundary conditions, due to the complex definition of these boundary conditions. Since various boundary conditions for the LBM [29–31] are provided, enabling analysis of diverse fluid flow problems, previous optimization methods employing the LBM must be expanded so that any desired boundary condition of the LBM can be treated in the optimization problem. In other words, the adjoint boundary conditions should be theoretically derived under the framework of sensitivity analysis based on the adjoint variable method.

To overcome the problem of how to incorporate the LBM boundary conditions in optimization problems, we propose a new sensitivity analysis based on the ALBM, in which we use the discrete velocity Boltzmann equation with the BGK approximation. Since the discrete velocity Boltzmann equation incorporates discrete particle velocities but continuous space and time, the various boundary conditions for the LBM can be easily introduced, and the adjoint equation can be analytically derived and discretized based on the strategy used in the ALBM [22,23].

Here, we apply the proposed methodology to isothermal- and thermal-fluid flow optimization problems in which prescribed flow velocity, pressure, temperature, and adiabatic boundary conditions are treated as representative boundary conditions in the LBM. Details of the sensitivity analysis dealing with these boundary conditions are provided to confirm the applicability of the proposed sensitivity analysis. Based on our new formulations, we construct a topology optimization method for the design of a flow channel in which the pressure drop minimization and heat exchange maximization problems are formulated. In the following sections, the basic concept of the LBM is discussed first. Next, the topology optimization problems are formulated for the pressure drop minimization and heat exchange maximization problems, and the procedures used in each sensitivity analysis based on the discrete velocity Boltzmann equation are described in detail. The numerical implementations and optimization algorithms are then explained and, finally, we introduce several numerical examples to confirm the utility of the proposed method.

## 2. Lattice Boltzmann method

### 2.1. Basic equation

We now discuss the concept of the LBM that will be applied here to an incompressible viscous fluid while considering the temperature field. In the following, we use the dimensionless variables defined in Appendix A. The basic idea of the LBM is that the fluid regime is represented as an aggregation of fictitious particles, which makes it possible to obtain macroscopic variables such as the fluid velocity, pressure, and temperature, from the moments of the velocity distribution functions that express the distribution state of the particles.

In the LBM, we consider a modeled fluid, which is composed of identical particles whose velocities are restricted to a finite set of $q$ vectors, $\boldsymbol{c}_1, \boldsymbol{c}_2, \ldots, \boldsymbol{c}_q$. If we use the BGK approximation [24] for collision terms, the behavior of the particles is described by the following discrete velocity Boltzmann equations:

$$Sh\frac{\partial f_i}{\partial t} + \boldsymbol{c}_i \cdot \nabla f_i = -\frac{1}{\varepsilon_f}(f_i - f_i^{\mathrm{eq}}), \tag{1}$$

where $f_i$ is the velocity distribution function, $f_i^{\mathrm{eq}}$ is the local equilibrium distribution function given later, $\varepsilon_f$ is a dimensionless parameter of the same order as the Knudsen number, and $Sh = \hat{U}/\hat{c}$ is the Strouhal number of $O(\varepsilon_f)$. Note that $1/\varepsilon_f$ in Eq. (1) corresponds to the frequency of the collision between the particles. Also, it should be noted that the Strouhal number appears in Eq. (1) because we have two scales for a characteristic speed: one is a particle speed $\hat{c}$ which is of the order of sound speed, and the other is a flow speed $\hat{U}$ which is of $O(1)$. In this study, we employ the two-dimensional nine-velocity (D2Q9) model (Fig. 1), which has the following velocity vectors:

$$[\boldsymbol{c}_1, \boldsymbol{c}_2, \boldsymbol{c}_3, \boldsymbol{c}_4, \boldsymbol{c}_5, \boldsymbol{c}_6, \boldsymbol{c}_7, \boldsymbol{c}_8, \boldsymbol{c}_9] = \begin{bmatrix} 0 & 1 & 0 & -1 & 0 & 1 & -1 & -1 & 1 \\ 0 & 0 & 1 & 0 & -1 & 1 & 1 & -1 & -1 \end{bmatrix}. \tag{2}$$

To formulate the LBE, the discrete velocity Boltzmann equation is discretized with respect to a position $\boldsymbol{x}$ and time $t$ using a lattice spacing $\Delta x$ and a time step $\Delta t$. Performing the same discretization as in [32], we obtain the following LBE for fluid flows:

$$f_i(\boldsymbol{x} + \boldsymbol{c}_i\Delta x, t + \Delta t) = f_i(\boldsymbol{x}, t) - \frac{1}{\tau_f}\{f_i(\boldsymbol{x}, t) - f_i^{\mathrm{eq}}(\boldsymbol{x}, t)\}, \tag{3}$$

where $\tau_f = \varepsilon_f/\Delta x$ is the dimensionless relaxation time and of $O(1)$, which is related to the viscosity of the fluid given below. Note that the time step $\Delta t$ is chosen so that the particles exactly travel the lattice spacing. Thus, $\Delta\hat{t} = \Delta\hat{x}/\hat{c}$ in the dimensional form; it follows that $\Delta t = Sh\Delta x$. In the same way, the evolution of the distribution function $g_i$ representing the temperature $T$ is described as follows:

$$g_i(\boldsymbol{x} + \boldsymbol{c}_i\Delta x, t + \Delta t) = g_i(\boldsymbol{x}, t) - \frac{1}{\tau_g}\{g_i(\boldsymbol{x}, t) - g_i^{\mathrm{eq}}(\boldsymbol{x}, t)\}, \tag{4}$$

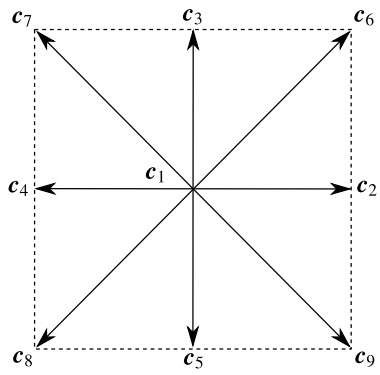


**Fig. 1.** Particle velocity vectors $\boldsymbol{c}_i$ of D2Q9 model.

where $\tau_g = \varepsilon_g/\Delta x$, in which $\varepsilon_g$ represents a dimensionless parameter of the same order as the Knudsen number, is also the dimensionless relaxation time and of $O(1)$, which is related to the thermal diffusivity of the fluid given below. The equilibrium distribution functions, $f_i^{\mathrm{eq}}$ and $g_i^{\mathrm{eq}}$, are given by

$$f_i^{\mathrm{eq}} = E_i \rho \left\{ 1 + 3\boldsymbol{c}_i \cdot \boldsymbol{u} + \frac{9}{2}(\boldsymbol{c}_i \cdot \boldsymbol{u})^2 - \frac{3}{2}|\boldsymbol{u}|^2 \right\}, \tag{5}$$

$$g_i^{\mathrm{eq}} = E_i T \left(1 + 3\boldsymbol{c}_i \cdot \boldsymbol{u}\right). \tag{6}$$

For the D2Q9 model, the weight $E_i$ is defined as follows:

$$E_i = \begin{cases} 4/9 & \text{for } i = 1 \\ 1/9 & \text{for } i = 2, 3, 4, 5 \\ 1/36 & \text{for } i = 6, 7, 8, 9. \end{cases} \tag{7}$$

The density $\rho$, the fluid velocity $\boldsymbol{u}$, the temperature $T$, and the heat flux $\boldsymbol{q}_T$ are obtained from the moments of the velocity distribution functions, as follows:

$$\rho = \sum_{i=1}^{9} f_i, \tag{8}$$

$$\boldsymbol{u} = \frac{1}{\rho} \sum_{i=1}^{9} \boldsymbol{c}_i f_i, \tag{9}$$

$$T = \sum_{i=1}^{9} g_i, \tag{10}$$

$$\boldsymbol{q}_T = \sum_{i=1}^{9} \boldsymbol{c}_i g_i - T\boldsymbol{u}. \tag{11}$$

When using the D2Q9 model, the pressure $p$ is represented as follows:

$$p = \frac{\rho}{3}. \tag{12}$$

Applying the asymptotic theory [33] to Eqs. (3) and (4), Inamuro et al. [32] verified that the macroscopic variables in Eqs. (8)–(10) and (12) satisfy the following macroscopic equations, with relative errors of $O[(\Delta x)^2]$,

$$\nabla \cdot \boldsymbol{u} = 0, \tag{13}$$

$$Sh\frac{\partial \boldsymbol{u}}{\partial t} + (\boldsymbol{u} \cdot \nabla)\boldsymbol{u} = -\nabla p + \nu \nabla^2 \boldsymbol{u}, \tag{14}$$

$$Sh\frac{\partial T}{\partial t} + (\boldsymbol{u} \cdot \nabla)T = \alpha_T \nabla^2 T, \tag{15}$$

which represent the continuity equation (13), the NSE (14), and the convection–diffusion equation (15) for the temperature, respectively. The kinematic viscosity $\nu$ and the thermal diffusivity $\alpha_T$ of the fluid are given by

$$\nu = \frac{1}{3}\left(\tau_f - \frac{1}{2}\right)\Delta x, \tag{16}$$

$$\alpha_T = \frac{1}{3}\left(\tau_g - \frac{1}{2}\right)\Delta x. \tag{17}$$

When an external body force $\boldsymbol{F}(\boldsymbol{x}, t)$ and heat source $Q_T(\boldsymbol{x}, t)$ are applied, the evolution equations in Eqs. (3) and (4) can be computed in a stepwise fashion as follows:

*Step 1.* $f_i$ and $g_i$ are evolved without the body force and the heat source, by the following equations:

$$f_i^*(\boldsymbol{x} + \boldsymbol{c}_i\Delta x, t + \Delta t) = f_i(\boldsymbol{x}, t) - \frac{1}{\tau_f}\{f_i(\boldsymbol{x}, t) - f_i^{\mathrm{eq}}(\boldsymbol{x}, t)\}, \tag{18}$$

$$g_i^*(\boldsymbol{x} + \boldsymbol{c}_i\Delta x, t + \Delta t) = g_i(\boldsymbol{x}, t) - \frac{1}{\tau_g}\{g_i(\boldsymbol{x}, t) - g_i^{\mathrm{eq}}(\boldsymbol{x}, t)\}. \tag{19}$$

*Step 2.* $f_i$ and $g_i$ are corrected as follows:

$$f_i(\boldsymbol{x}, t + \Delta t) = f_i^*(\boldsymbol{x}, t + \Delta t) + 3\Delta x E_i \boldsymbol{c}_i \cdot \boldsymbol{F}(\boldsymbol{x}, t + \Delta t), \tag{20}$$

$$g_i(\boldsymbol{x}, t + \Delta t) = g_i^*(\boldsymbol{x}, t + \Delta t) + \Delta x E_i Q_T(\boldsymbol{x}, t + \Delta t). \tag{21}$$

### 2.2. Initial and boundary conditions for the LBM

Since problems formulated with the LBM include initial and boundary conditions, values for these conditions must be provided, to enable computation of the time evolution of the velocity distribution function. In this study, we assume that the initial values of the particle distribution functions are those of the equilibrium distribution functions, given initial values of $\rho(\boldsymbol{x}, 0)$, $\boldsymbol{u}(\boldsymbol{x}, 0)$, and $T(\boldsymbol{x}, 0)$, as follows:

$$f_i(\boldsymbol{x}, 0) = f_i^{\mathrm{eq}}(\rho(\boldsymbol{x}, 0), \boldsymbol{u}(\boldsymbol{x}, 0)), \tag{22}$$

$$g_i(\boldsymbol{x}, 0) = g_i^{\mathrm{eq}}(T(\boldsymbol{x}, 0), \boldsymbol{u}(\boldsymbol{x}, 0)), \tag{23}$$

On the other hand, the boundary conditions applied in the LBM are generally more complex than those in a conventional numerical scheme. Due to the characteristics of the particle propagations formulated in the LBE, the boundary values of the velocity distribution functions that satisfy $\boldsymbol{n} \cdot \boldsymbol{c}_i < 0$ (where $\boldsymbol{n}$ is the outward normal vector) are unknown, and must be specified so that boundary conditions for the macroscopic flow, such as no-slip, or prescribed velocity or pressure boundary conditions, are adequately represented. For instance, in Fig. 1, if the $x$–$y$ plane is defined so that $\boldsymbol{c}_1 = (0, 0)^{\mathrm{T}}$ is the origin of the coordinate axis and the fluid domain is defined such that $y > 0$, the velocity distribution functions $f_3$, $f_6$ and $f_7$ must be specified based on known values of $f_1$, $f_2$, $f_4$, $f_5$, $f_8$, and $f_9$ (and $g_i$ must also be treated in the same manner as $f_i$). A no-slip boundary condition, which implies that $\boldsymbol{u} = \boldsymbol{0}$ on wall boundary $\Gamma_{\mathrm{W}}$, can be represented using the following simple exchange of the unknown $f_i$ to the known $f_i$:

$$\left.\begin{aligned} f_3 &= f_5 \\ f_6 &= f_8 \\ f_7 &= f_9 \end{aligned}\right\} \quad \text{on } \Gamma_{\mathrm{W}}. \tag{24}$$

This is the so-called bounce back boundary condition [15], which is easy to implement in the LBM code and is often used to impose a no-slip boundary condition.

To treat the prescribed velocity boundary condition, Zhou and He [28] proposed the following boundary conditions:

$$\left.\begin{aligned} f_3 &= f_5 + \tfrac{2}{3}\rho v_0 \\ f_6 &= f_8 + \tfrac{1}{6}\rho v_0 - \tfrac{1}{2}(f_2 - f_4) \\ f_7 &= f_9 + \tfrac{1}{6}\rho v_0 + \tfrac{1}{2}(f_2 - f_4) \end{aligned}\right\} \quad \text{on } \Gamma_{\mathrm{V}}, \text{ and } \rho = \frac{f_1 + f_2 + f_4 + 2(f_5 + f_8 + f_9)}{1 - v_0}, \tag{25}$$

where $v_0$ represents the prescribed velocity in the $y$-direction on boundary $\Gamma_{\mathrm{V}}$. Similarly, a prescribed density boundary condition, based on the pressure boundary condition arising from the relationship expressed in Eq. (12), can be introduced by using the following equations:

$$\left.\begin{aligned} f_3 &= f_5 + \tfrac{2}{3}\rho_0 v \\ f_6 &= f_8 + \tfrac{1}{6}\rho_0 v - \tfrac{1}{2}(f_2 - f_4) \\ f_7 &= f_9 + \tfrac{1}{6}\rho_0 v + \tfrac{1}{2}(f_2 - f_4) \end{aligned}\right\} \quad \text{on } \Gamma_{\mathrm{P}}, \text{ and } v = 1 - \frac{f_1 + f_2 + f_4 + 2(f_5 + f_8 + f_9)}{\rho_0}, \tag{26}$$

where $\rho_0$ represents the prescribed density on boundary $\Gamma_{\mathrm{P}}$.

For a thermal-fluid flow problem, an adiabatic boundary condition can be imposed by using the following equations [32,34]:

$$\left.\begin{aligned} g_3 &= \tfrac{1}{9}T(1+3v) \\ g_6 &= \tfrac{1}{36}T(1+3v) \\ g_7 &= \tfrac{1}{36}T(1+3v) \end{aligned}\right\} \text{ on } \Gamma_{\mathrm{A}}, \text{ and } T = \frac{6(g_5+g_8+g_9)}{1-3v}. \tag{27}$$

Likewise, a prescribed temperature boundary condition can be introduced by using the following equations:

$$\left.\begin{aligned} g_3 &= \tfrac{1}{9}T(1+3v) \\ g_6 &= \tfrac{1}{36}T(1+3v) \\ g_7 &= \tfrac{1}{36}T(1+3v) \end{aligned}\right\} \text{ on } \Gamma_{\mathrm{T}}, \text{ and } T = \frac{6\{T_0-(g_1+g_2+g_4+g_5+g_8+g_9)\}}{1+3v}, \tag{28}$$

where $T_0$ represents the prescribed temperature.

We note that the boundary conditions in Eqs. (24)–(28) above will be used in the formulations of the optimization problems described in Section 3.2.

## 3. Formulation of topology optimization problems

### 3.1. Topology optimization

Consider a structural optimization problem to determine the boundary of a design domain, $\Omega$, in which the objective function that expresses the intended performance of the target system is to be minimized, or maximized, based on optimization theories. The basic concept of topology optimization is the introduction of a fixed design domain $D$ that includes the original design domain, i.e., $\Omega \subset D$, and the use of the characteristic function $\chi$ in order to replace the original structural optimization problem with a material distribution problem in the fixed design domain. Let $\chi$ be the characteristic function, defined as

$$\chi(\boldsymbol{x}) := \begin{cases} 1 & \text{if } \boldsymbol{x} \in \Omega \\ 0 & \text{if } \boldsymbol{x} \in D \setminus \Omega, \end{cases} \tag{29}$$

where $\boldsymbol{x}$ represents a position in the fixed design domain $D$. Since this characteristic function can be highly discontinuous, some relaxation technique must be introduced for the numerical treatment.

In the density approach, the characteristic function, $\chi(\boldsymbol{x})$, is typically replaced with a relaxed function, $\gamma(\boldsymbol{x})$, which is treated as the design variable in topology optimization problems, and belongs to the following set,

$$\mathcal{X}_{\mathrm{ad}} = \left\{ \gamma \in L^{\infty}(D) \,|\, 0 \leqslant \gamma \leqslant 1, \text{ a.e. in } D \right\}. \tag{30}$$

### 3.2. Optimization problems

Here, we formulate the topology optimization problems for the design of a flow channel and use the LBM to compute fluid flows under a low Reynolds number condition. In this paper, two optimization problems are treated: 1) a pressure drop minimization problem under isothermal fluid flow, and 2) a heat exchange maximization problem under thermal fluid flow.

#### 3.2.1. Pressure drop minimization problem

First, we formulate the pressure drop minimization problem for the design of a flow channel that can efficiently transport fluid between an inlet and an outlet in an internal flow system. A schematic diagram of this problem is shown in Fig. 2, where the completely fluid domain $\Omega$ is defined such that $\gamma = 1$ in the design variable, and the completely solid domain $D \setminus \Omega$ is defined as $\gamma = 0$. The inlet boundary condition is set to the prescribed velocity, i.e., $\boldsymbol{u} = \boldsymbol{u}_{\mathrm{in}}$ at $\Gamma_{\mathrm{V}}$, and the outlet boundary condition is set to the prescribed pressure, i.e., $p = p_{\mathrm{out}}$ at $\Gamma_{\mathrm{P}}$. Here, to represent both fluid and solid domains, we employ the typical way proposed by Borravall and Petersson [6], in which the fixed design domain is defined as a porous medium, based on Darcy's law. Thus, we introduce the body force $\boldsymbol{F}$, as follows:

$$\boldsymbol{F} = -\alpha_{\gamma}\boldsymbol{u}, \tag{31}$$

where $\alpha_{\gamma}$ is defined as

$$\alpha_{\gamma} = \alpha_{\max} + (\alpha_{\min} - \alpha_{\max})\frac{\gamma(1+q)}{\gamma+q}, \tag{32}$$

where $q$ is a tuning parameter to control the convexity of $\alpha_{\gamma}$, and we set this parameter to $q = 0.1$. Since the material distribution of fluid and solid domains is represented using the porous model, $\alpha_{\gamma}$ is the so-called inverse permeability, as defined in Eq. (32). $\gamma = 0$ corresponds to a solid domain $D \setminus \Omega$ that is represented as having zero permeability, i.e.,

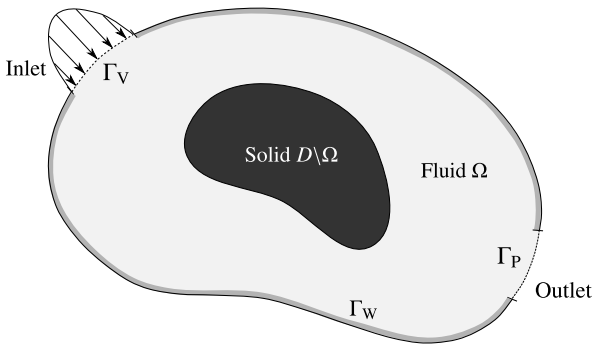


**Fig. 2.** Schematic figure of fixed design domain $D$ and its boundary settings.

$\alpha_{\max} \to \infty$, and $\gamma = 1$ corresponds to a fluid domain $\Omega$ that is represented as having infinite permeability, i.e., $\alpha_{\min} = 0$. We note that a sufficiently large value must be chosen as $\alpha_{\max}$ in the numerical computation, to model the no-slip boundary condition in the fixed design domain $D$.

Based on the above formulation, the fluid flow in $D$ is governed by the following problem concerning the initial and boundary values:

$$\left\{\begin{array}{l} \left.\begin{array}{l} \nabla\cdot\boldsymbol{u} = 0 \\ Sh\frac{\partial \boldsymbol{u}}{\partial t} + (\boldsymbol{u}\cdot\nabla)\boldsymbol{u} = -\nabla p + \nu\nabla^2\boldsymbol{u} - \alpha_\gamma \boldsymbol{u} \end{array}\right\} \text{Governing equations in } D \\ \left.\begin{array}{ll} \boldsymbol{u} = \boldsymbol{0} & \text{on } \Gamma_W \\ \boldsymbol{u} = \boldsymbol{u}_{\text{in}} & \text{on } \Gamma_V \\ p = p_{\text{out}} & \text{on } \Gamma_P \end{array}\right\} \text{Boundary conditions} \quad \left.\begin{array}{l} \boldsymbol{u}(\boldsymbol{x},0) = \boldsymbol{u}^{\text{ini}}(\boldsymbol{x}) \\ p(\boldsymbol{x},0) = p^{\text{ini}}(\boldsymbol{x}) \end{array}\right\} \text{Initial conditions,} \end{array}\right. \tag{33}$$

where $\boldsymbol{u}^{\text{ini}}(\boldsymbol{x})$ and $p^{\text{ini}}(\boldsymbol{x})$ represent the initial values of the fluid velocity and pressure, respectively.

As a result, the pressure drop minimization problem can be formulated as follows:

$$\left\{\begin{array}{ll} \inf\limits_{\gamma\in\mathcal{X}_{\text{ad}}} & J_1 = \int_I \int_{\Gamma_V} p\,\mathrm{d}\Gamma\mathrm{d}t - \int_I \int_{\Gamma_P} p\,\mathrm{d}\Gamma\mathrm{d}t \\ \text{s.t.} & V = \int_D \gamma\,\mathrm{d}\Omega - V_{\max}\int_D \mathrm{d}\Omega \leqslant 0 \\ & \boldsymbol{u} \text{ and } p \text{ satisfy the initial–boundary value problem in Eq. (33),} \end{array}\right. \tag{34}$$

where $J_1$ represents the objective functional corresponding to the pressure drop between the inlet and the outlet, and $V$ represents the volume constraint, where $V_{\max}$ is the volume ratio of fluid with respect to the volume of $D$. $I := [0, t_{\text{f}}]$ represents the observation time interval of the fluid flow, with the final time $t_{\text{f}}$ that can be given as an arbitrary value. We note that the fluid velocity and pressure are calculated using the LBM in our study. That is, the initial–boundary value problem in Eq. (33) is solved using the LBM, whereas the FEM is typically used in previous studies dealing with the pressure drop minimization problem. We also note that the above optimization problem is formulated as a time-dependent problem, whereas in most previous studies, a steady-state condition is considered. This is because the LBM is used for computing the time-dependent fluid flow, so it is appropriate to formulate the optimization problem as a time-dependent problem. It should be noted that the above formulation can be used for solving not only time-dependent optimization problems, but also steady-state problems under sufficiently low Reynolds number conditions.

*3.2.2. Heat exchange maximization problem*

The second problem we formulate is to maximize heat exchange for a flow channel design that can be applied for cooling devices such as a heat sink. Here, we consider the design domain shown in Fig. 2. A heat source $Q_T$ is defined in the solid domain $D\backslash\Omega$ and the aim is to find an optimal configuration of the flow channel so that the coolant flow removes a maximal amount of heat input through an area of the solid domain. The boundary conditions for $\boldsymbol{u}$ and $p$ are same as those applied in the pressure drop minimization problem. Additionally, the adiabatic boundary condition, $\boldsymbol{n}\cdot\nabla T = 0$, and the prescribed temperature condition, $T = T_{\text{in}}$, are imposed at $\Gamma_W \cup \Gamma_P$, and $\Gamma_V$, respectively.

Based on previous research dealing with heat exchange maximization problems [35,36], we introduce the heat generation coefficient $\beta_\gamma$, which is dependent on design variable $\gamma$, as follows:

$$Q_T = \beta_\gamma(1 - T), \tag{35}$$

where $\beta_\gamma$ is defined as

$$\beta_\gamma = \beta_{\max} + (\beta_{\min} - \beta_{\max})\frac{\gamma(1+q)}{\gamma+q}. \tag{36}$$

We note that since the dimensionless temperature $T$ is normalized according to the value of the reference temperature $\hat{T}_{\mathrm{ref}}$, the heat source $Q_T$ restricts the maximum value of dimensional temperature so that $\hat{T} \approx \hat{T}_{\mathrm{ref}}$, which corresponds to a maximum value for dimensionless temperature of $T = 1$. Due to the definition of $\beta_\gamma$ in Eq. (36), the maximum value of heat generation coefficient $\beta_{\max}$ is given in the solid domain corresponding to $\gamma = 0$, while the minimum value of heat generation coefficient $\beta_{\min}$ is given in the fluid domain corresponding to $\gamma = 1$. In this study, the minimum value of heat generation coefficient is set to $\beta_{\min} = 0$.

Based on the above formulation, the thermal-fluid flow in $D$ is governed by the following problem concerning the initial and boundary values:

$$\left\{\begin{array}{l} \nabla\cdot\boldsymbol{u}=0 \\ Sh\frac{\partial \boldsymbol{u}}{\partial t}+(\boldsymbol{u}\cdot\nabla)\boldsymbol{u}=-\nabla p+\nu\nabla^2\boldsymbol{u}-\alpha_\gamma\boldsymbol{u} \\ Sh\frac{\partial T}{\partial t}+(\boldsymbol{u}\cdot\nabla)T=\alpha_T\nabla^2 T+\beta_\gamma(1-T) \end{array}\right\} \text{ Governing equations in } D$$

$$\left\{\begin{array}{ll} \boldsymbol{u}=\boldsymbol{0} & \text{on } \Gamma_{\mathrm{W}} \\ \boldsymbol{u}=\boldsymbol{u}_{\mathrm{in}} & \text{on } \Gamma_{\mathrm{V}} \\ p=p_{\mathrm{out}} & \text{on } \Gamma_{\mathrm{P}} \\ \boldsymbol{n}\cdot\nabla T=0 & \text{on } \Gamma_{\mathrm{W}}\cup\Gamma_{\mathrm{P}} \\ T=T_{\mathrm{in}} & \text{on } \Gamma_{\mathrm{V}} \end{array}\right\} \text{ Boundary conditions} \qquad \left\{\begin{array}{l} \boldsymbol{u}(\boldsymbol{x},0)=\boldsymbol{u}^{\mathrm{ini}}(\boldsymbol{x}) \\ p(\boldsymbol{x},0)=p^{\mathrm{ini}}(\boldsymbol{x}) \\ T(\boldsymbol{x},0)=T^{\mathrm{ini}}(\boldsymbol{x}) \end{array}\right\} \text{ Initial conditions,} \tag{37}$$

where $T^{\mathrm{ini}}(\boldsymbol{x})$ represents the initial temperature value.

Based on a previous study [35], the heat exchange maximization problem can be formulated as

$$\left\{\begin{array}{ll} \inf\limits_{\gamma\in\mathcal{X}_{\mathrm{ad}}} & J_2=-\int_I\int_D \beta_\gamma(1-T)\,\mathrm{d}\Omega\mathrm{d}t \\ \text{s.t.} & P=\int_I\int_{\Gamma_{\mathrm{V}}} p\,\mathrm{d}\Gamma\mathrm{d}t-\int_I\int_{\Gamma_{\mathrm{P}}} p\,\mathrm{d}\Gamma\mathrm{d}t-\eta_{\max}\Delta p^{\mathrm{init}}\leqslant 0 \\ & \boldsymbol{u},\ p,\ \text{and } T \text{ satisfy the initial–boundary value problem in Eq. (37),} \end{array}\right. \tag{38}$$

where $J_2$ is the objective functional that corresponds to the total amount of heat exchanged in the fixed design domain and $P$ is an inequality constraint that limits the maximum pressure drop based on the value of an initial pressure drop, $\Delta p^{\mathrm{init}}$, obtained after computing the first optimization step. The parameter $\eta_{\max}$ is used for determining the maximum pressure drop in the fluidic system. In this optimization problem, we note that $P$ is an essential constraint that prevents optimal configurations from having channels with infinitesimal widths, which would be allowed in the absence of a pressure drop constraint, due to the occurrence of infinite pressure drops [17,37,38].

As with the above pressure drop minimization problem, the fluid velocity, pressure and temperature are calculated using the LBM. That is, the initial–boundary value problem in Eq. (37) is solved using the LBM in this study.

## 4. Sensitivity analysis based on the discrete velocity Boltzmann equation

Based on the ALBM [22,23], we now consider the strategy for deriving the design sensitivities for the optimization problems discussed in Section 3. The ALBM is based on the use of the LBM to compute the fluid flow in fluid optimization problems, and its key idea is that design sensitivities are derived using the adjoint variable method in which the Boltzmann equation is employed to formulate the Lagrangian. Based on the continuous adjoint approach, the adjoint equation is derived as an equation that closely resembles the Boltzmann equation, and is solved using the LBM. As a result, both the state and adjoint fields can be solved using the same efficient algorithm of the LBM, and the design sensitivities are obtained with a fully explicit calculation.

In our previous research [25], we used the ALBM and demonstrated its applicability to topology optimization problems. Since boundary conditions when using the LBM are included in the equations for unknown velocity distribution functions, such as Eqs. (24)–(28), the ALBM, in which the Lagrangian is formulated using the Boltzmann equation, cannot be used because complex boundary conditions, such as the inlet and outlet boundary conditions in Eqs. (25) and (26), cannot be introduced. This means that boundary conditions for the adjoint equation, corresponding to the complex boundary conditions, cannot be imposed. Although simple inlet and outlet boundary conditions, such as $f = f^{\mathrm{eq}}$ at the inlet and outlet, were used in our previous research [25], these are rarely used in research dealing with the LBM due to the poor accuracy of the solutions of the NSE.

To overcome this restriction, in the method proposed here, we formulate the optimization problem using the discrete velocity Boltzmann equation in Eq. (1) that includes the position $\boldsymbol{x}$, time $t$, and discrete particle velocities $\boldsymbol{c}_i$. Since the discrete velocity Boltzmann equation is only discretized with respect to the particle velocities, the various boundary conditions required in the LBM can be easily introduced and the adjoint equation can be systematically derived and discretized based on the strategy used in the ALBM.

The design sensitivity we consider in this paper is the gradient of the objective functional, $J_n$ ($n = 1, 2$), with respect to the design variable $\gamma$. The design sensitivity is defined as the Gâteaux derivative, $\langle J_n', \delta\gamma\rangle$, given by

$$\langle J_n', \delta\gamma \rangle = \frac{\mathrm{d}}{\mathrm{d}\varrho} J_n(\gamma + \varrho\delta\gamma)\bigg|_{\varrho=0}, \tag{39}$$

where $\delta\gamma$ is an arbitrary function.

### 4.1. Sensitivity analysis for pressure drop minimization problem

First, we discuss the sensitivity analysis for the pressure drop minimization problem formulated in (34). To conduct the sensitivity analysis based on the ALBM incorporating the discrete velocity Boltzmann equation, the Lagrange multiplier method is employed, using Lagrange multipliers $\tilde{f}_i = \tilde{f}_i(\boldsymbol{x}, t)$, and the Lagrangian, $\bar{J}_1$, is defined as follows:

$$\bar{J}_1 = J_1 + R_1, \tag{40}$$

where $R_1$ is defined as

$$R_1 = \int_I \int_D \sum_{i=1}^{9} \tilde{f}_i \left\{ Sh \frac{\partial f_i}{\partial t} + \boldsymbol{c}_i \cdot \nabla f_i + \frac{1}{\varepsilon_f} \left( f_i - f_i^{\mathrm{eq}} \right) + 3\alpha_\gamma E_i \boldsymbol{c}_i \cdot \boldsymbol{u} \right\} \mathrm{d}\Omega\mathrm{d}t. \tag{41}$$

To introduce the initial and boundary conditions, Eq. (41) is rewritten as

$$\begin{aligned} R_1 = {} & \int_D \sum_{i=1}^{9} \left[ Sh f_i \tilde{f}_i \right]_{t_0}^{t_1} \mathrm{d}\Omega + \int_I \int_\Gamma \sum_{i=1}^{9} (\boldsymbol{c}_i \cdot \boldsymbol{n}) f_i \tilde{f}_i \mathrm{d}\Gamma\mathrm{d}t \\ & + \int_I \int_D \sum_{i=1}^{9} f_i \left\{ -Sh \frac{\partial \tilde{f}_i}{\partial t} - \boldsymbol{c}_i \cdot \nabla \tilde{f}_i + \frac{1}{\varepsilon_f} \left( \tilde{f}_i - \tilde{f}_i^{\mathrm{eq}} \right) + 3\alpha_\gamma E_i \boldsymbol{c}_i \cdot \tilde{\boldsymbol{m}} \right\} \mathrm{d}\Omega\mathrm{d}t, \end{aligned} \tag{42}$$

where $\tilde{\boldsymbol{m}} = \sum_{i=1}^{9} E_i \boldsymbol{c}_i \tilde{f}_i$. The Gâteaux derivative of $\bar{J}_1$ with respect to $\gamma$ can be derived as

$$\begin{aligned} \langle \bar{J}_1', \delta\gamma \rangle = {} & \int_I \int_{\Gamma_{\mathrm{V}}} \sum_{i=1}^{9} \frac{1}{3} \delta f_i \mathrm{d}\Gamma\mathrm{d}t - \int_I \int_{\Gamma_{\mathrm{P}}} \sum_{i=1}^{9} \frac{1}{3} \delta f_i \mathrm{d}\Gamma\mathrm{d}t \\ & + \int_D \sum_{i=1}^{9} Sh \delta f_i(t_1) \tilde{f}_i(t_1) \mathrm{d}\Omega + \int_I \int_\Gamma \sum_{i=1}^{9} (\boldsymbol{c}_i \cdot \boldsymbol{n}) \delta f_i^{\mathrm{b}} \tilde{f}_i \mathrm{d}\Gamma\mathrm{d}t \\ & + \int_I \int_D \sum_{i=1}^{9} \delta f_i \left\{ -Sh \frac{\partial \tilde{f}_i}{\partial t} - \boldsymbol{c}_i \cdot \nabla \tilde{f}_i + \frac{1}{\varepsilon_f} \left( \tilde{f}_i - \tilde{f}_i^{\mathrm{eq}} \right) + 3\alpha_\gamma E_i \boldsymbol{c}_i \cdot \tilde{\boldsymbol{m}} \right\} \mathrm{d}\Omega\mathrm{d}t \\ & + \int_I \int_D \left( 3\alpha_\gamma \boldsymbol{u} \cdot \tilde{\boldsymbol{m}} \right) \delta\gamma \mathrm{d}\Omega\mathrm{d}t, \end{aligned} \tag{43}$$

where $\delta f_i = (\partial f_i / \partial \gamma)\delta\gamma$, and $\tilde{f}_i^{\mathrm{eq}}$ is defined as

$$\tilde{f}_i^{\mathrm{eq}} = \tilde{\rho} + 3(\boldsymbol{c}_i - \boldsymbol{u}) \cdot \tilde{\boldsymbol{j}}, \tag{44}$$

where $\tilde{\rho}$, and $\tilde{\boldsymbol{j}}$ are defined as follows [39]:

$$\tilde{\rho} = \sum_{j=1}^{9} E_j \tilde{f}_j \left( 1 + 3\boldsymbol{c}_j \cdot \boldsymbol{u} + \frac{9}{2} \boldsymbol{\mathcal{H}}_j^{(2)} : (\boldsymbol{u} \otimes \boldsymbol{u}) \right), \tag{45}$$

$$\tilde{\boldsymbol{j}} = \sum_{j=1}^{9} E_j \tilde{f}_j \left( \boldsymbol{c}_j + 3\boldsymbol{\mathcal{H}}_j^{(2)} \boldsymbol{u} \right), \tag{46}$$

where "$\otimes$", and ":" represent the tensor product and the tensor inner product, respectively. $\boldsymbol{\mathcal{H}}_j^{(2)}$ represents the second Hermite polynomial in the discrete case, $\boldsymbol{\mathcal{H}}_j^{(2)} = \boldsymbol{c}_j \otimes \boldsymbol{c}_j - 3\boldsymbol{\delta}$, with the Kronecker delta, $\boldsymbol{\delta}$. From the fifth term of the right-hand side in Eq. (43), the adjoint equation can be immediately derived as

$$-Sh \frac{\partial \tilde{f}_i}{\partial t} - \boldsymbol{c}_i \cdot \nabla \tilde{f}_i = -\frac{1}{\varepsilon_f} \left( \tilde{f}_i - \tilde{f}_i^{\mathrm{eq}} \right) - 3\alpha_\gamma E_i \boldsymbol{c}_i \cdot \tilde{\boldsymbol{m}}. \tag{47}$$

In addition, the initial conditions can be obtained using the third term of the right-hand side in Eq. (43), as follows:

$$\tilde{f}_i(t_\mathrm{f}) = 0. \tag{48}$$

Next, the boundary conditions for the adjoint equation are derived using the first, second, and fourth terms in Eq. (43) for boundaries $\Gamma_\mathrm{W}$, $\Gamma_\mathrm{V}$, and $\Gamma_\mathrm{P}$, respectively. The key point guiding the derivations of the boundary conditions is the handling of $\delta f_i^\mathrm{b}$ in the fourth term of the right-hand side in Eq. (43). The detailed process for deriving the adjoint boundary conditions is described in Appendix B, and these are finally obtained as follows:

$$\left.\begin{aligned}\tilde{f}_5 &= \tilde{f}_3\\ \tilde{f}_8 &= \tilde{f}_6\\ \tilde{f}_9 &= \tilde{f}_7\end{aligned}\right\} \quad \text{on } \Gamma_\mathrm{W}, \tag{49}$$

$$\left.\begin{aligned}\tilde{f}_5 &= -\tfrac{2}{3(1-v_0)} + \tilde{f}_3 + \tfrac{v_0}{3(1-v_0)}\left(4\tilde{f}_3 + \tilde{f}_6 + \tilde{f}_7\right)\\ \tilde{f}_8 &= -\tfrac{2}{3(1-v_0)} + \tilde{f}_6 + \tfrac{v_0}{3(1-v_0)}\left(4\tilde{f}_3 + \tilde{f}_6 + \tilde{f}_7\right)\\ \tilde{f}_9 &= -\tfrac{2}{3(1-v_0)} + \tilde{f}_7 + \tfrac{v_0}{3(1-v_0)}\left(4\tilde{f}_3 + \tilde{f}_6 + \tilde{f}_7\right)\end{aligned}\right\} \quad \text{on } \Gamma_\mathrm{V}, \tag{50}$$

$$\left.\begin{aligned}\tilde{f}_5 &= \tilde{f}_3 - \tfrac{1}{3}\left(4\tilde{f}_3 + \tilde{f}_6 + \tilde{f}_7\right)\\ \tilde{f}_8 &= \tilde{f}_6 - \tfrac{1}{3}\left(4\tilde{f}_3 + \tilde{f}_6 + \tilde{f}_7\right)\\ \tilde{f}_9 &= \tilde{f}_7 - \tfrac{1}{3}\left(4\tilde{f}_3 + \tilde{f}_6 + \tilde{f}_7\right)\end{aligned}\right\} \quad \text{on } \Gamma_\mathrm{P}. \tag{51}$$

We note that these adjoint boundary conditions resemble the specific boundary conditions applied in the LBM, due to the use in the ALBM of the discrete velocity Boltzmann equation instead of the Boltzmann equation.

Consequently, the design sensitivity of this optimization problem is obtained from Eq. (43), as follows:

$$\langle \bar{J}_1', \delta\gamma \rangle = \int_I \int_D \left(3\alpha_\gamma' \boldsymbol{u}\cdot\tilde{\boldsymbol{m}}\right)\delta\gamma \,\mathrm{d}\Omega\mathrm{d}t, \tag{52}$$

with

$$\alpha' = (\alpha_\mathrm{min} - \alpha_\mathrm{max})\left(1 - \frac{\gamma}{\gamma+q}\right)\frac{1+q}{\gamma+q}. \tag{53}$$

### 4.2. Sensitivity analysis for heat exchange maximization problem

Next, we discuss the sensitivity analysis for the heat exchange maximization problem formulated in Eq. (38). The basic procedure for conducting the sensitivity analysis is similar to that used in the above pressure drop minimization problem, but the Lagrangian with respect to $J_2$ is formulated here using the augmented Lagrange multiplier method (e.g. [40]), which enables the inequality constraint $P$ to be precisely imposed on the optimization problem. We use the Lagrange multipliers $\tilde{g}_i = \tilde{g}_i(\boldsymbol{x}, t)$ and $\mu$, and a penalty parameter $\sigma$. Consequently, the Lagrangian, $\bar{J}_2$, is defined as follows:

$$\bar{J}_2 = J_2 + R_1 + R_2 + \frac{1}{2\sigma}\left\{(\max\{0, \mu + \sigma P\})^2 - \mu^2\right\}, \tag{54}$$

where $R_1$ is as defined in Eq. (41) above, and $R_2$ is defined as

$$R_2 = \int_I \int_D \sum_{i=1}^{9} \tilde{g}_i \left\{Sh\frac{\partial g_i}{\partial t} + \boldsymbol{c}_i\cdot\nabla g_i + \frac{1}{\varepsilon_g}\left(g_i - g_i^\mathrm{eq}\right) - \beta_\gamma(1+\tilde{T})\right\}\mathrm{d}\Omega\mathrm{d}t. \tag{55}$$

In this study, we set the value of penalty parameter to $\sigma = 1.0\times10^{-2}$. Since the design sensitivity of $\bar{J}_2$ is derived using $\langle \bar{J}_2', \delta\gamma\rangle$ in the same manner as for $\langle \bar{J}_1', \delta\gamma\rangle$, the adjoint equation for $\tilde{g}_i$ can be derived as follows:

$$-Sh\frac{\partial \tilde{g}_i}{\partial t} - \boldsymbol{c}_i\cdot\nabla\tilde{g}_i = -\frac{1}{\varepsilon_g}\left(\tilde{g}_i - \tilde{g}_i^\mathrm{eq}\right) + \beta_\gamma(1+\tilde{T}), \tag{56}$$

where $\tilde{g}_i^\mathrm{eq}$ is defined as

$$\tilde{g}_i^\mathrm{eq} = \tilde{T} + 3\boldsymbol{u}\cdot\tilde{\boldsymbol{q}}, \tag{57}$$

where $\tilde{T}$ and $\tilde{\boldsymbol{q}}$ are defined as follows:

$$\tilde{T} = \sum_{i=1}^{9} E_i \tilde{g}_i, \tag{58}$$

$$\tilde{\boldsymbol{q}} = \sum_{i=1}^{9} E_i \boldsymbol{c}_i \tilde{g}_i. \tag{59}$$

On the other hand, based on Eq. (47), the adjoint equation for $\tilde{f}_i$ is defined as follows:

$$-Sh\frac{\partial \tilde{f}_i}{\partial t} - \boldsymbol{c}_i \cdot \nabla \tilde{f}_i = -\frac{1}{\varepsilon_f}\left(\tilde{f}_i - \tilde{f}_i^{\mathrm{eq}}\right) - 3\alpha_\gamma E_i \boldsymbol{c}_i \cdot \tilde{\boldsymbol{m}} + G_i^f, \tag{60}$$

where $G_i^f$ is derived from the derivative of $E_2$ with respect to $f_i$, and is defined as

$$G_i^f = \frac{3T}{\rho \varepsilon_g}(\boldsymbol{c}_i - \boldsymbol{u}) \cdot \tilde{\boldsymbol{q}}. \tag{61}$$

In addition, the initial conditions applied in Eq. (56) are defined as follows:

$$\tilde{g}_i(t_{\mathrm{f}}) = 0. \tag{62}$$

Based on the derivation strategy for the boundary conditions discussed in Section 4.1, the boundary conditions corresponding to Eqs. (27) and (28) can be derived as follows:

$$\left.\begin{aligned} \tilde{g}_5 &= \tfrac{1+3v}{6(1-3v)}(4\tilde{g}_3 + \tilde{g}_6 + \tilde{g}_7) \\ \tilde{g}_8 &= \tfrac{1+3v}{6(1-3v)}(4\tilde{g}_3 + \tilde{g}_6 + \tilde{g}_7) \\ \tilde{g}_9 &= \tfrac{1+3v}{6(1-3v)}(4\tilde{g}_3 + \tilde{g}_6 + \tilde{g}_7) \end{aligned}\right\} \text{ on } \Gamma_{\mathrm{W}} \cup \Gamma_{\mathrm{P}}, \tag{63}$$

$$\left.\begin{aligned} \tilde{g}_5 &= -\tfrac{1}{6}(4\tilde{g}_3 + \tilde{g}_6 + \tilde{g}_7) \\ \tilde{g}_8 &= -\tfrac{1}{6}(4\tilde{g}_3 + \tilde{g}_6 + \tilde{g}_7) \\ \tilde{g}_9 &= -\tfrac{1}{6}(4\tilde{g}_3 + \tilde{g}_6 + \tilde{g}_7) \end{aligned}\right\} \text{ on } \Gamma_{\mathrm{V}}. \tag{64}$$

Again, the details of the derivation process for these boundary conditions are described in Appendix C.

As a result, the design sensitivity for this optimization problem is defined as follows:

$$\langle \bar{J}_2', \delta\gamma \rangle = \int_I \int_D \left\{ 3\alpha_\gamma' \boldsymbol{u} \cdot \tilde{\boldsymbol{m}} + \beta_\gamma'(1-T)(1+\tilde{T}) \right\} \delta\gamma \, \mathrm{d}\Omega \mathrm{d}t, \tag{65}$$

with

$$\beta' = (\beta_{\min} - \beta_{\max})\left(1 - \frac{\gamma}{\gamma+q}\right)\frac{1+q}{\gamma+q}. \tag{66}$$

## 5. Numerical implementation

### 5.1. Optimization algorithm

The optimization algorithm of the proposed method is now described.

*Step 1.* The initial values of the state, adjoint, and design variables are set throughout the fixed design domain $D$.
*Step 2.* The LBE for the pressure drop minimization problem, or the heat exchange maximization problem, is calculated until a steady-state condition is satisfied.
*Step 3.* If the criteria of the objective functional and inequality constraint are satisfied, an optimal configuration is obtained and the optimization is finished, otherwise the adjoint equations are calculated and the procedure advances to Step 4.
*Step 4.* The design sensitivities $\bar{J}_n'$ are calculated using the current state and adjoint variables.
*Step 5.* The design variable is updated using the method of moving asymptotes (MMA) [41], after which the optimization procedure returns to Step 2 of the iterative loop.

The MMA constructs a sequence of convex separable sub-problems that are solved by the primal–dual method, which ensures that the Karush–Kuhn–Tucker conditions are satisfied. This algorithm is suited for nonlinear optimization problems with a large number of design variables and few constraints, and is known to be very efficient for topology optimization problems.

In addition, these procedures are iterated until the following criterion for the value of the objective functional is met:

$$\left| \frac{J_n^N - J_n^{N-1}}{J_n^N} \right| < \epsilon_{\mathrm{opt}}, \tag{67}$$

where superscript $N$ represents the number of iterations carried out during the optimization process. We set the value of this criterion so that $\epsilon_{\mathrm{opt}} = 1.0 \times 10^{-4}$. In addition, we employ the following criteria for judging the steady-state condition:

$$\left\| \frac{\boldsymbol{u}^N - \boldsymbol{u}^{N-1}}{\boldsymbol{u}^N} \right\|_{L^2(D)} < \epsilon_u, \tag{68}$$

$$\left\| \frac{\boldsymbol{q}_T^N - \boldsymbol{q}_T^{N-1}}{\boldsymbol{q}_T^N} \right\|_{L^2(D)} < \epsilon_q, \tag{69}$$

where $\epsilon_u$ and $\epsilon_q$ represent the judgment criteria for the steady-state condition of fluid velocity and heat flux, respectively. We set the values of these criteria so that $\epsilon_u = \epsilon_q = 1.0 \times 10^{-4}$. We note that the criteria represented in Eqs. (68) and (69) must be simultaneously satisfied to obtain an optimal configuration in the heat exchange maximization problem, whereas only the criterion represented in Eq. (68) is considered in the pressure drop minimization problem.

Since the state variables must be recorded for all time steps when the ALBM is used to solve the adjoint problem that includes state variables, memory requirements will be prohibitive in many practical engineering problems if data for all time steps are preserved. Fortunately, in steady-state problems, each converged state and adjoint value at each optimization step $N$ can be used as an initial value when calculating the time evolution equations in next optimization step. Since the state and adjoint equations are formulated as an explicit scheme, the calculations at each optimization step rapidly converge except for the first optimization step. Although the use of this numerical technique is only allowed in steady-state problems, the characteristics of the explicit scheme are highly advantageous and enable an optimal configuration to be obtained quickly [26]. Similarly, the design sensitivities are calculated using only each converged value of the state and adjoint variables, whereas the time integral is contained in the original definition of the sensitivities in Eqs. (52) and (65).

In addition, we note that employing a filtering technique to preserve the smoothness of the design variables or design sensitivities during the optimization process is unnecessary here. This is because none of the design sensitivities given by Eqs. (52) and (65) contain a derivative in their integrands. A filtering technique, e.g. [42], can, of course, be used to avoid the dependency of optimal configurations with respect to the mesh discretization of the design domain. However, since such numerical treatment often causes difficulty in setting certain parameters, we do not employ a filter in this study.

### 5.2. Adjoint lattice Boltzmann equation

Due to the similarity between the configuration of the discrete velocity Boltzmann equations and that of the adjoint equations represented in Section 4, which is a consequence of the discretization strategy used in the LBM, the adjoint equations can also be discretized as simple time evolution equations. That is, the adjoint problem based on the LBM in the pressure drop minimization problem can be formulated as follows:

$$\begin{cases} \tilde{f}_i^*(\boldsymbol{x} - \boldsymbol{c}_i \Delta x, t - \Delta t) = \tilde{f}_i(\boldsymbol{x}, t) - \frac{1}{\tau_f}\{\tilde{f}_i(\boldsymbol{x}, t) - \tilde{f}_i^{\mathrm{eq}}(\boldsymbol{x}, t)\} \\ \tilde{f}_i(\boldsymbol{x}, t - \Delta t) = \tilde{f}_i^*(\boldsymbol{x}, t - \Delta t) - 3\Delta x \alpha_\gamma(\boldsymbol{x}) E_i \boldsymbol{c}_i \cdot \tilde{\boldsymbol{m}}(\boldsymbol{x}, t - \Delta t) \\ \tilde{f}_i(\boldsymbol{x}, t_{\mathrm{f}}) = 0 \qquad \text{(Initial condition)} \\ \tilde{f}_i(\boldsymbol{x}, t) = \tilde{f}_i^{\mathrm{b}}(\boldsymbol{x}, t) \quad \text{(Boundary condition)}, \end{cases} \tag{70}$$

where

$$\tilde{f}_{5,8,9}^{\mathrm{b}} = \begin{cases} \tilde{f}_{3,6,7} & \text{on } \Gamma_{\mathrm{W}} \\ \tilde{f}_{3,6,7} - \frac{2}{3(1-v_0)} + \frac{v_0}{3(1-v_0)}\left(4\tilde{f}_3 + \tilde{f}_6 + \tilde{f}_7\right) & \text{on } \Gamma_{\mathrm{V}} \\ \tilde{f}_{3,6,7} - \frac{1}{3}(4\tilde{f}_3 + \tilde{f}_6 + \tilde{f}_7) & \text{on } \Gamma_{\mathrm{P}}, \end{cases} \tag{71}$$

where $\tilde{f}_i^{\mathrm{b}}$ represents the boundary values based on Eqs. (49), (50), and (51) that express the boundary conditions for $\tilde{f}_i$ at $y = 0$ in Fig. 1, in which the analysis domain is located in $y \geqslant 0$ and the unknown values are $\tilde{f}_5$, $\tilde{f}_8$, and $\tilde{f}_9$. We note that the unknown values of the adjoint problem at the $y = 0$ boundary are different from those of the state problem, in which the unknown values are $f_3$, $f_6$, and $f_7$. The unknown state values are in diametrically opposite locations with respect to those of the adjoint variables. For the other boundaries, e.g., the boundary at which $x = 0$ and the analysis domain is located in $x \geqslant 0$ in Fig. 1, the unknown values of the state variables are $f_2$, $f_6$, and $f_9$, and correspond to the unknown values of the adjoint variables $f_4$, $f_8$, and $f_7$, respectively. We note that the boundary conditions for the adjoint equations at each boundary must be individually derived.

Similarly, the adjoint problem based on the LBM in the heat exchange maximization problem can be formulated as follows:

$$\begin{cases} \tilde{f}_i^*(\boldsymbol{x}-\boldsymbol{c}_i\Delta x, t-\Delta t) = \tilde{f}_i(\boldsymbol{x},t) - \frac{1}{\tau_f}\{\tilde{f}_i(\boldsymbol{x},t) - \tilde{f}_i^{\mathrm{eq}}(\boldsymbol{x},t)\} + \frac{3T}{\rho\tau_g}(\boldsymbol{c}_i - \boldsymbol{u})\cdot\tilde{\boldsymbol{q}} \\ \tilde{f}_i(\boldsymbol{x}, t-\Delta t) = \tilde{f}_i^*(\boldsymbol{x}, t-\Delta t) - 3\Delta x\alpha_\gamma(\boldsymbol{x})E_i\boldsymbol{c}_i\cdot\tilde{\boldsymbol{m}}(\boldsymbol{x}, t-\Delta t) \\ \tilde{f}_i(\boldsymbol{x}, t_{\mathrm{f}}) = 0 \qquad \text{(Initial condition)} \\ \tilde{f}_i(\boldsymbol{x}, t) = \tilde{f}_i^{\mathrm{b}}(\boldsymbol{x}, t) \quad \text{(Boundary condition)}, \end{cases} \tag{72}$$

$$\begin{cases} \tilde{g}_i^*(\boldsymbol{x}-\boldsymbol{c}_i\Delta x, t-\Delta t) = \tilde{g}_i(\boldsymbol{x},t) - \frac{1}{\tau_g}\{\tilde{g}_i(\boldsymbol{x},t) - \tilde{g}_i^{\mathrm{eq}}(\boldsymbol{x},t)\} \\ \tilde{g}_i(\boldsymbol{x}, t-\Delta t) = \tilde{g}_i^*(\boldsymbol{x}, t-\Delta t) + \Delta x\beta_\gamma(\boldsymbol{x})\{1+\tilde{T}(\boldsymbol{x}, t-\Delta t)\} \\ \tilde{g}_i(\boldsymbol{x}, t_{\mathrm{f}}) = 0 \qquad \text{(Initial condition)} \\ \tilde{g}_i(\boldsymbol{x}, t) = \tilde{g}_i^{\mathrm{b}}(\boldsymbol{x}, t) \quad \text{(Boundary condition)}, \end{cases} \tag{73}$$

where

$$\tilde{f}_{5,8,9}^{\mathrm{b}} = \begin{cases} \tilde{f}_{3,6,7} & \text{on } \Gamma_{\mathrm{W}} \\ \tilde{f}_{3,6,7} - \frac{2(\max\{0,\mu+\sigma P\})}{3(1-v_0)} + \frac{v_0}{3(1-v_0)}\left(4\tilde{f}_3 + \tilde{f}_6 + \tilde{f}_7\right) & \text{on } \Gamma_{\mathrm{V}} \\ \tilde{f}_{3,6,7} - \frac{1}{3}(4\tilde{f}_3 + \tilde{f}_6 + \tilde{f}_7) - \frac{12T(1+3v)}{\rho_0(1-3v)}(4\tilde{g}_3 + \tilde{g}_6 + \tilde{g}_7) & \text{on } \Gamma_{\mathrm{P}}, \end{cases} \tag{74}$$

$$\tilde{g}_{5,8,9}^{\mathrm{b}} = \begin{cases} \frac{1+3v}{6(1-3v)}(4\tilde{g}_3 + \tilde{g}_6 + \tilde{g}_7) & \text{on } \Gamma_{\mathrm{W}} \cup \Gamma_{\mathrm{P}} \\ -\frac{1}{6}(4\tilde{g}_3 + \tilde{g}_6 + \tilde{g}_7) & \text{on } \Gamma_{\mathrm{V}}. \end{cases} \tag{75}$$

These discretized adjoint equations allow us to avoid having to deal with matrix operations when obtaining design sensitivities during the optimization process.

## 6. Numerical examples

Here, we confirm the utility of our proposed method. In all the numerical examples, the reference length and speed are defined as the inlet width and inlet mean velocity magnitude, respectively. Using the kinematic viscosity in Eq. (16), the thermal diffusivity $\alpha_T$ in Eq. (17), and the dimensionless values of the inlet length $L$ and mean velocity magnitude $U$, the Reynolds number $Re$ and the Prandtl number $Pr$ are defined as

$$Re = \frac{LU}{\nu}, \tag{76}$$

$$Pr = \frac{\nu}{\alpha_T}. \tag{77}$$

For all numerical examples, the initial conditions for the fluid velocity, density, and temperature are set so that $\boldsymbol{u}(\boldsymbol{x}, 0) = 0$, $\rho(\boldsymbol{x}, 0) = 1$ (corresponding to $p(\boldsymbol{x}, 0) = 1/3$), and $T(\boldsymbol{x}, 0) = 1$, respectively. Based on the initial conditions for $f_i$ and $g_i$ in Eqs. (22) and (23), the velocity distribution functions are $f_i(\boldsymbol{x}, 0) = g_i(\boldsymbol{x}, 0) = E_i$.

### 6.1. Validation of the adjoint sensitivity

First, the design sensitivities, computed using the proposed sensitivity analysis, were compared with the outcome of finite difference approximations, as shown in Fig. 3. The evaluation nodes illustrated in this figure were selected in the design domain, which is discretized using a $100\Delta x \times 100\Delta x$ grid and contains a cylinder with a radius of $15\Delta x$ at the center of the design domain. The design variables were set so that $\gamma = 0.1$ for the cylinder and $\gamma = 0.9$ elsewhere. The finite differences, $J'_{\mathrm{FD}n}$, were computed using the central difference scheme, as follows:

$$J'_{\mathrm{FD}n} = \frac{J_n(\gamma+\epsilon) - J_n(\gamma-\epsilon)}{2\epsilon}, \tag{78}$$

where $\epsilon$ is set to a small positive value. We can validate the adjoint model if and only if the adjoint sensitivity and finite difference sensitivity in Eq. (78) are equal.

Here, the Reynolds number and the Prandtl number were set so that $Re = 10$ and $Pr = 6$, respectively, when computing the adjoint sensitivities $\bar{J}'_n$ and the finite difference approximations $J'_{\mathrm{FD}n}$. Fig. 4 illustrates that the proposed method computes sensitivities that are in good agreement with the finite differences except when $\epsilon$ is set to too small a value, both in the pressure drop minimization problem and the heat exchange maximization problem. We note that the observed

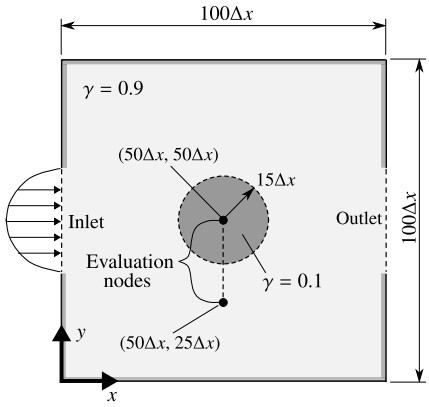


**Fig. 3.** Analysis domain for the validation of design sensitivity. The analysis domain was discretized using a $100\Delta x \times 100\Delta x$ grid, and includes a centrally placed circle of radius $15\Delta x$. The design variables in the fluid and solid domains were set with $\gamma = 0.9$ and 0.1, respectively. The finite difference sensitivities were evaluated at 25 evaluation nodes, spaced $\Delta x$ apart, between $(x, y) = (50\Delta x, 25\Delta x)$ and $(x, y) = (50\Delta x, 50\Delta x)$.

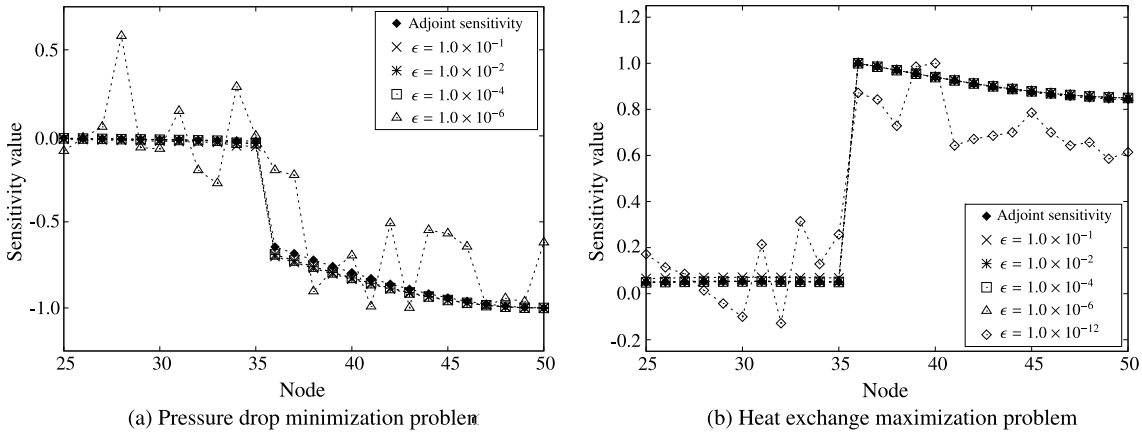


**Fig. 4.** Comparison of the finite difference approximations $J'_{\mathrm{FD}_n}$ with respect to the adjoint sensitivities $\bar{J}'_n$: (a) pressure drop minimization problem; (b) heat exchange maximization problem. The values are normalized using each maximum absolute value. The nodes ranging along the horizontal axis correspond to evaluation nodes in the analysis domain shown in Fig. 3.

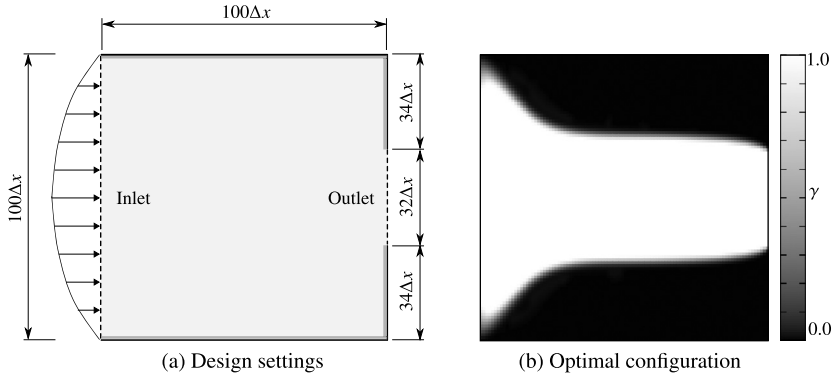


**Fig. 5.** Pressure drop minimization problem: (a) design settings, (b) optimal configuration (black: solid, white: fluid).

numerical instabilities were due to machine precision errors. The results allow us to confirm that appropriate values of the adjoint sensitivities were obtained.

Next, we further confirm the validity of the adjoint sensitivity by applying it to the diffuser problem shown in Fig. 5, which is often treated as a benchmark problem in topology optimization for the pressure drop minimization problems [6,16,26,27,43,44].

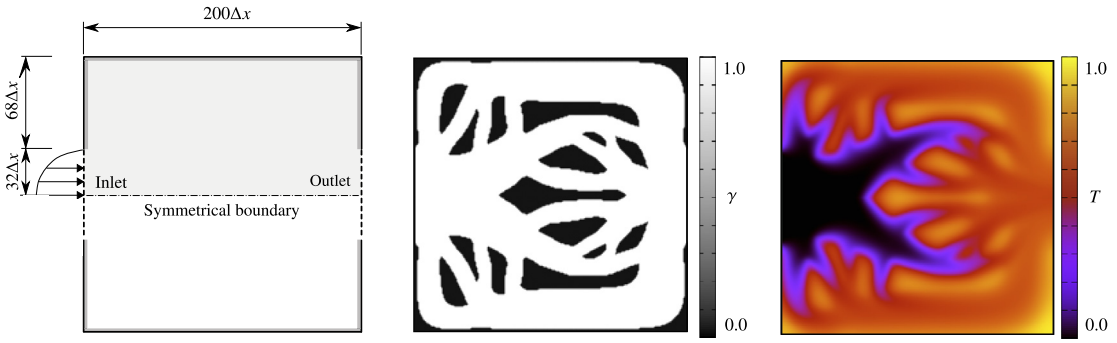


(a) Design settings (b) Optimal configuration (c) Temperature distribution

**Fig. 6.** Heat exchange maximization problem: (a) design settings, (b) optimal configuration (black: solid, white: fluid), (c) temperature distribution.

As shown in Fig. 5(a), the analysis domain is discretized using a $100\Delta x \times 100\Delta x$ grid, and the volume constraint is set so that $V_{\max} = 0.5$. Since previous studies on this diffuser problem developed methodologies for Stokes flow, or very low Reynolds number flow, we set our fluidic system to a low Reynolds number flow, with $Re = 1$, to enable a valid comparison. The following settings were used: $L = 100\Delta x$, $U = 1.0 \times 10^{-3}$, and $\tau_f = 0.8$. The prescribed pressure at the outlet boundary was set to $p_0 = \rho_0/3$ where $\rho_0 = 1.0$. The maximum value of inverse permeability was set to $\alpha_{\max} = 4.0 \times 10^2$.

Fig. 5(b) shows the optimal configuration obtained with the proposed method, and its close similarity to the configuration obtained by Borrvall and Petersson [6] confirms that it can obtain appropriate results. Although the dissipation energy is generally used for the objective functional when formulating a fluid flow optimization problem, the pressure drop is considered to be essentially equivalent to the dissipation energy [45,46] under low Reynolds number flows, where the loss of dynamic pressure and the effect of body force can be safely ignored [16].

### 6.2. Heat exchange maximization problem

We now confirm the utility of the proposed method by applying it to a heat sink design problem, which is also treated in previous studies [35,36]. As shown in Fig. 6(a), the analysis domain is discretized using a $200\Delta x \times 100\Delta x$ grid, and a symmetrical boundary condition is imposed. The initial design variable value is set to $\gamma = 1$ in the fixed design domain $D$. The inlet temperature is set to $T_0 = 0$ and the outlet pressure is set to $p_0 = \rho_0/3$, with $\rho_0 = 1.0$. The maximum value of inverse permeability was set to $\alpha_{\max} = 2.0 \times 10^2$.

Figs. 6(b) and (c) show the optimal configuration and temperature distribution for parameter settings of $Re = 7$, $Pr = 6$, $\eta_{\max} = 10$, and $\beta_{\max} = 0.1$. The optimization history of the design variable $\gamma$ is illustrated in Fig. 7, and the convergence histories of the objective functional and the pressure drop are shown in Fig. 8, in which both values are monotonically converged by approximately the 350th step. The optimal configuration is an appropriately complex channel that is suitable for efficient heat exchange between the fluid and solid domains. The complexity of the channel suggests that a large surface area between the fluid and solid domains is advantageous for heat exchange. This characteristic, of optimal configurations composed of geometrically complex channels, was also revealed in previous studies [35,36].

#### 6.2.1. Dependency of optimal configuration on $\eta_{\max}$

As described above, inequality constraint $P$ is an essential constraint that prevents the optimal configuration from including channels with infinitesimal widths. For this reason, we investigated the effect of $\eta_{\max}$ settings on the optimal configuration.

Fig. 9 shows the optimal results when parameter $\eta_{\max}$ is set to 5, 10, and 20. The different values of $\eta_{\max}$ result in dramatically different optimal configurations, and indicate that the allowable maximum value of the pressure drop greatly affects the geometrical complexity. That is, when the value of $\eta_{\max}$ is small, the result is a geometrically simple channel configuration, whereas a larger value of $\eta_{\max}$ produces a much more complex configuration. Table 1 shows the objective functional values for the three $\eta_{\max}$ settings at their respective final optimization steps. We can confirm that the proposed method enables a quantitative control of the maximum pressure drop in an optimal configuration, by setting an appropriate value of $\eta_{\max}$.

#### 6.2.2. Dependency of optimal configuration on $\beta_{\max}$

Here, we investigate the effect of $\beta_{\max}$ settings on the optimal configuration. Fig. 10(a) shows the optimal configurations for different $\beta_{\max}$ settings: $\beta_{\max} = 0.01,\ 0.1,\ 0.3$. Additionally, the temperature distributions for each $\beta_{\max}$ setting are shown in Figs. 10(b), (c), and (d).

Fig. 10(a) clearly shows that the value of $\beta_{\max}$ greatly affects the geometrical complexity of the optimal configuration. Table 2 shows the crosscheck of objective functional values for the different optimal configurations and $\beta_{\max}$ settings. For

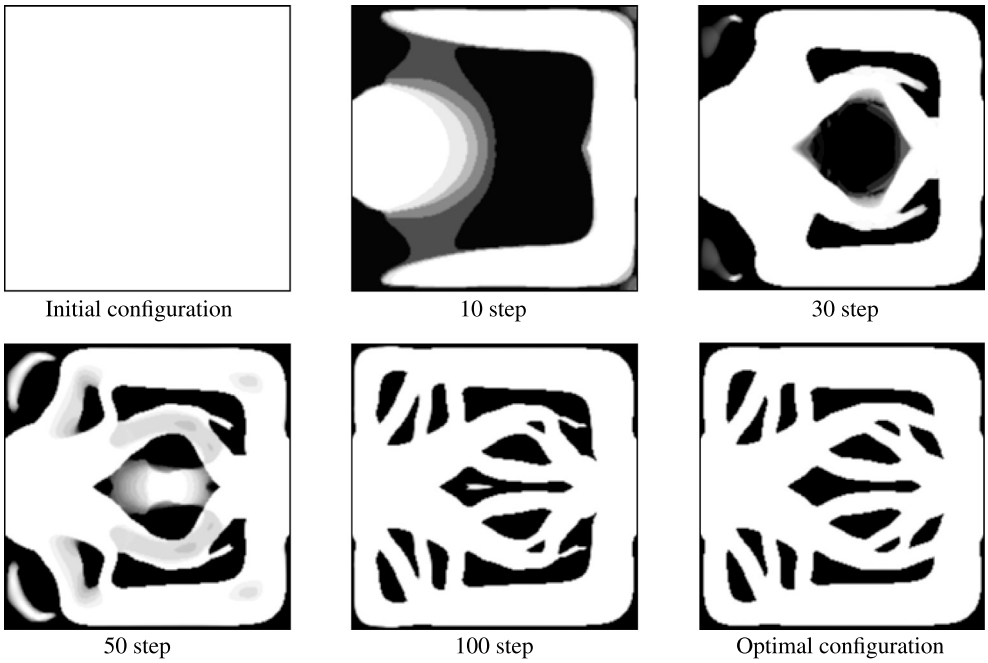


**Fig. 7.** Optimization history of design variable for the heat exchange maximization problem.

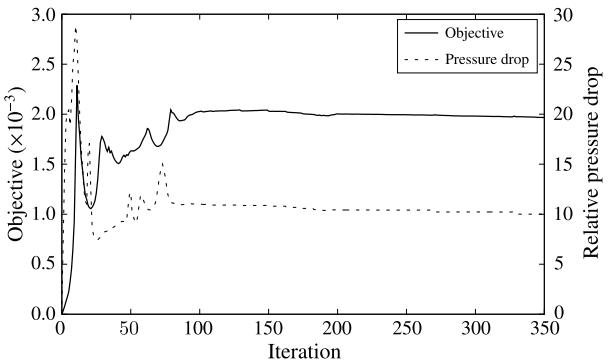


**Fig. 8.** Convergence histories of the objective functional $J_2$ and the relative pressure drop $\Delta p/\Delta p^{\text{init}}$, with $\Delta p$ representing the current pressure drop.

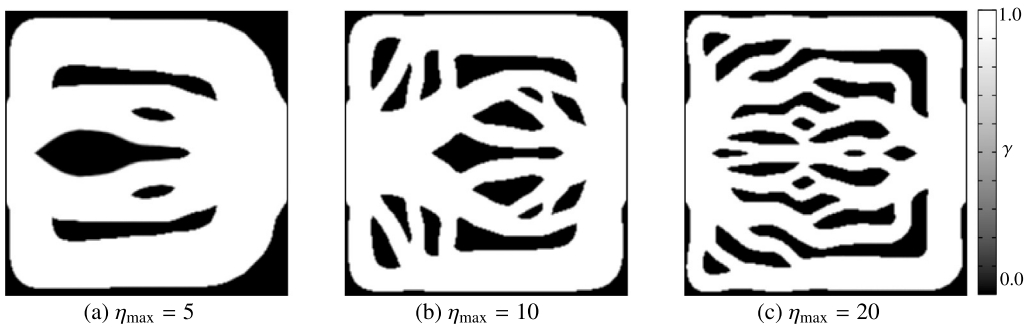


**Fig. 9.** Effect of parameter $\eta_{\max}$ settings on optimal configurations: (a) $\eta_{\max} = 5$, (b) $\eta_{\max} = 10$, (c) $\eta_{\max} = 20$.

the crosscheck, the optimal configurations were analyzed across the different $\beta_{\max}$ settings, and we can confirm that the configuration that is optimized for a certain flow condition is better than the others for its particular flow condition.

$\beta_{\max}$ is the coefficient that controls the heat generation according to the temperature difference. Thus, setting a large $\beta_{\max}$ value corresponds to the characteristic of a solid domain that is difficult to cool. In fact, as shown in Figs. 10(b), (c), and (d), we observe that temperatures in the solid domains tend to be high when $\beta_{\max}$ is set to a large value. Given

**Table 1**
Values of objective functional and relative pressure drop for different $\eta_{\max}$ settings in the heat exchange maximization problem.

| $\eta_{\max}$ | 5 | 10 | 20 |
|---|---|---|---|
| Objective functional ($\times 10^{-3}$) | 1.41 | 1.96 | 2.34 |
| Relative pressure drop | 5.00 | 9.99 | 19.97 |

**Table 2**
Crosscheck of objective functional values ($\times 10^{-3}$) for the heat exchange maximization problem shown in Fig. 10.

| Analysis $\beta_{\max}$ | Optimization $\beta_{\max}$ | | |
|---|---|---|---|
| | 0.01 | 0.1 | 0.3 |
| 0.01 | **0.63** | 1.61 | 1.91 |
| 0.1 | 0.50 | **1.96** | 2.46 |
| 0.3 | 0.37 | 1.81 | **2.50** |

**Table 3**
Relative volume of fluid, defined as $\int_D \gamma \, d\Omega / \int_D d\Omega$, for the optimal configurations in Fig. 10(a), when different $\beta_{\max}$ settings in the heat exchange maximization problem.

| $\beta_{\max}$ | 0.01 | 0.1 | 0.3 |
|---|---|---|---|
| Relative volume of fluid | 0.58 | 0.76 | 0.83 |

high temperatures in the solid domains, the optimal configuration when $\beta_{\max} = 0.3$ is set to a large value is complex, with many small islands of solid distributed so that a large surface area is obtained under the prescribed maximum pressure drop. Although one might imagine that having more islands of solid in the optimal configuration to increase the objective functional value would be an improvement, we note that this would violate the pressure drop constraint.

On the other hand, the optimal configuration when setting $\beta_{\max} = 0.01$ is geometrically simple, with only three large islands of solid. In this scenario, the total volume of solid domains takes precedence over the surface area, to increase the objective functional. Table 3 shows the fluid volume in the design domain for each optimal configuration shown in Fig. 10, and we observe that the fluid volume is increased as the value of $\beta_{\max}$ is increased. As shown in the left figure of 10(b), the interior of the solid domains are relatively cool due to the small value of $\beta_{\max}$, which corresponds to a small heat generation condition. On the other hand, when a larger value of $\beta_{\max}$ is set, as shown in the left figure in 10(d), the temperature distribution for the solid domains except in the vicinity of their boundaries is given as $T \approx 1$, which does not lead to improvement of the objective functional value. As a result, the optimal configurations shown in Fig. 10(a) can be viewed as being the most appropriate configurations for each flow condition.

## 7. Conclusion

This paper proposed a topology optimization method using the LBM incorporating a new sensitivity analysis based on the discrete velocity Boltzmann equation. The presented method was applied to pressure drop minimization and heat exchange maximization problems. We achieved the following:

(1) Two topology optimization problems were formulated: 1) pressure drop minimization problem, and 2) heat exchange maximization problem. The design sensitivities for these optimization problems were derived based on the ALBM, and we newly introduces a discrete velocity Boltzmann equation to formulate the Lagrangian, whereas the Boltzmann equation is used in the original ALBM. As a result, the accurate boundary conditions generally used in the LBM could be incorporated in the optimization problem formulations, and derivation of adjoint systems in which the adjoint boundary conditions reflect the boundary conditions of the LBM was enabled.
(2) An optimization algorithm was constructed based on the formulations of the optimization problems. Based on the ALBM, the use of the LBM discretization strategy allowed discretization of the adjoint equations as simple time evolution equations, in the same manner as that used for the LBE. Additionally, the converged state variable values and adjoint variable values at each optimization step were used as initial values when calculating the time evolution equations in the next optimization step, which greatly reduced computational cost.
(3) Numerical examples for two-dimensional problems were provided to confirm the utility of the proposed method. The proposed method obtained optimal configurations for the pressure drop minimization problem similar to those provided by an FEM-based method used in previous studies. In addition, optimal configurations for the heat exchange maximization problem were obtained, and we investigated the dependency of the optimal configurations with respect to settings of $\eta_{\max}$, used for controlling the pressure drop in the fluidic system. Based on our results, we clarified the relationship between $\eta_{\max}$ settings and the geometrical complexity of the optimal configurations. That is, setting $\eta_{\max}$ to a relatively

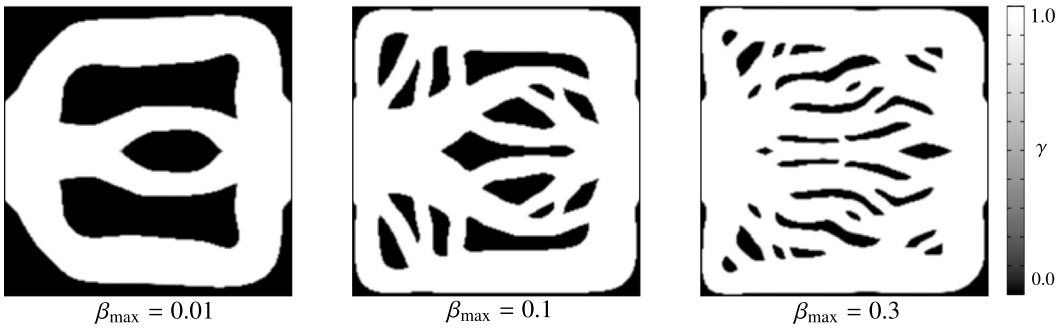


(a) Optimal configurations for different $\beta_{\max}$ values

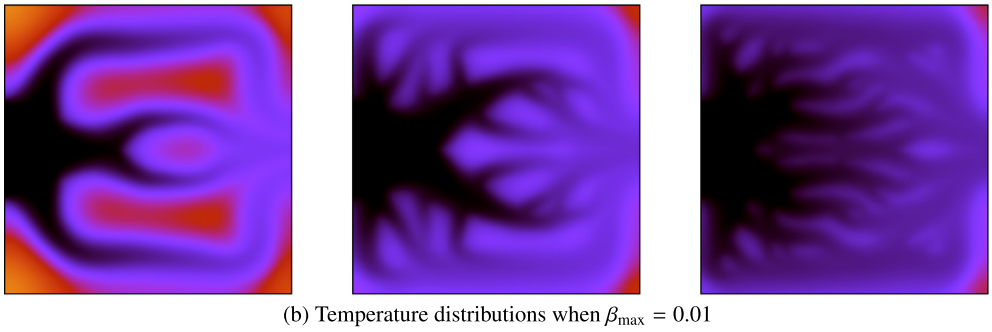

(b) Temperature distributions when $\beta_{\max} = 0.01$

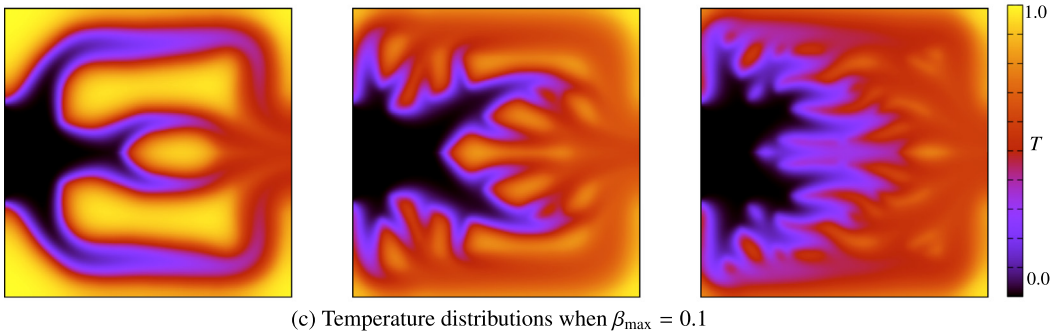


(c) Temperature distributions when $\beta_{\max} = 0.1$

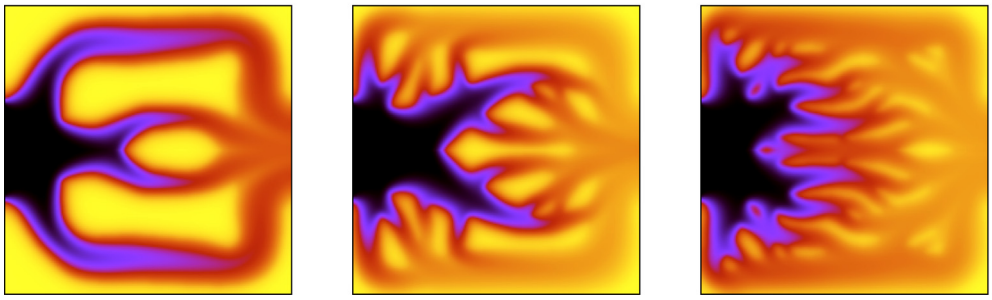

(d) Temperature distributions when $\beta_{\max} = 0.3$

**Fig. 10.** Effect of $\beta_{\max}$ settings on optimal configurations and the temperature distributions for different $\beta_{\max}$ settings: (a) Optimal configurations for different $\beta_{\max}$ values, (b) temperature distributions when $\beta_{\max} = 0.01$, (c) temperature distributions when $\beta_{\max} = 0.1$, and (d) temperature distributions when $\beta_{\max} = 0.3$.

large value leads to an optimal configuration that has a complex channel configuration, whereas a relatively small value of this parameter results in a simpler geometry. Furthermore, investigation of the effect of $\beta_{\max}$ settings on the optimal configurations showed that large $\beta_{\max}$ values resulted in configurations having a large number of small island domains, whereas small $\beta_{\max}$ values resulted in relatively simple configurations in which the volume of only a few solid domains was maximized. That is, an optimal configuration that has a large surface area is obtained when a relatively large $\beta_{\max}$ value is set, whereas a large solid volume is obtained when a relatively small $\beta_{\max}$ value is set, under the same pressure drop condition. These results indicate that the proposed method may be a useful basis for improving the optimal designs of flow channel devices such as heat sinks.

**Acknowledgements**

This work was supported by JSPS KAKENHI Grant Numbers 14J02008, 26820032.

## Appendix A. Definition of dimensionless variables

The dimensionless variables in this paper are defined in the following equations, using a reference length $\hat{L}$, a reference particle speed $\hat{c}$, a reference time $\hat{t}_{\mathrm{ref}} = \hat{L}/\hat{U}$, where $\hat{U}$ is a reference flow speed, a reference density $\hat{\rho}_{\mathrm{ref}}$, a reference temperature $\hat{T}_{\mathrm{ref}}$, and the specific heat at constant pressure $\hat{c}_p$, as follows:

$$\begin{cases} \boldsymbol{x} = \hat{\boldsymbol{x}}/\hat{L} & t = \hat{t}/\hat{t}_{\mathrm{ref}} & \Delta x = \Delta\hat{x}/\hat{L} & \Delta t = \Delta\hat{t}/\hat{t}_{\mathrm{ref}} \\ \boldsymbol{c}_i = \hat{\boldsymbol{c}}_i/\hat{c} & f_i = \hat{f}_i/\hat{\rho}_{\mathrm{ref}} & g_i = \hat{g}_i/\hat{T}_{\mathrm{ref}} & \rho = \hat{\rho}/\hat{\rho}_{\mathrm{ref}} \\ T = \hat{T}/\hat{T}_{\mathrm{ref}} & \boldsymbol{u} = \hat{\boldsymbol{u}}/\hat{c} & p = \hat{p}/(\hat{\rho}_{\mathrm{ref}}\hat{c}^2) & \boldsymbol{q}_T = \hat{\boldsymbol{q}}_T/(\hat{\rho}_{\mathrm{ref}}\hat{c}_p\hat{c}\hat{T}_{\mathrm{ref}}) \\ \nu = \hat{\nu}/(\hat{c}\hat{L}) & \alpha_T = \hat{\alpha}_T/(\hat{c}\hat{L}) & \alpha_\gamma = \hat{L}\hat{\alpha}_\gamma/(\hat{\rho}_{\mathrm{ref}}\hat{c}) & \beta_\gamma = \hat{L}\hat{\beta}_\gamma/\hat{c}. \end{cases} \tag{A.1}$$

Note that the circumflex represents “dimensional” entities.

## Appendix B. Derivation of the adjoint boundary conditions for the pressure drop minimization problem

First, the boundary condition for the no-slip boundary, $\Gamma_{\mathrm{W}}$, in Eq. (24) for the adjoint equation can be derived as follows:

$$\begin{aligned} \Theta_{\mathrm{W}} &= \int_I \int_{\Gamma_{\mathrm{W}}} \sum_{i=1}^{9} (\boldsymbol{c}_i \cdot \boldsymbol{n}) \delta f_i^{\mathrm{b}} \tilde{f}_i \mathrm{d}\Gamma \mathrm{d}t \\ &= \int_I \int_{\Gamma_{\mathrm{W}}} \left( -\tilde{f}_3 \delta f_3 + \tilde{f}_5 \delta f_5 - \tilde{f}_6 \delta f_6 - \tilde{f}_7 \delta f_7 + \tilde{f}_8 \delta f_8 + \tilde{f}_9 \delta f_9 \right) \mathrm{d}\Gamma \mathrm{d}t \\ &= \int_I \int_{\Gamma_{\mathrm{W}}} \left( -\tilde{f}_3 \delta f_5 + \tilde{f}_5 \delta f_5 - \tilde{f}_6 \delta f_8 - \tilde{f}_7 \delta f_9 + \tilde{f}_8 \delta f_8 + \tilde{f}_9 \delta f_9 \right) \mathrm{d}\Gamma \mathrm{d}t \\ &= \int_I \int_{\Gamma_{\mathrm{W}}} \left\{ (\tilde{f}_5 - \tilde{f}_3) \delta f_5 + (\tilde{f}_8 - \tilde{f}_6) \delta f_8 + (\tilde{f}_9 - \tilde{f}_7) \delta f_9 \right\} \mathrm{d}\Gamma \mathrm{d}t, \end{aligned} \tag{B.1}$$

where, since the boundary condition is defined so that Eq. (B.1) equals zero under $\delta f_{5,8,9} \neq 0$, we obtain the following boundary condition:

$$\left.\begin{aligned} \tilde{f}_5 &= \tilde{f}_3 \\ \tilde{f}_8 &= \tilde{f}_6 \\ \tilde{f}_9 &= \tilde{f}_7 \end{aligned}\right\} \quad \text{on } \Gamma_{\mathrm{W}}. \tag{B.2}$$

This is the same result as that of the previous research based on the ALBM [22,23] in which the Boltzmann equation with the BGK approximation was used to formulate the optimization problem. We note that Eq. (B.2) is used for the no-slip boundary condition, which is based on the bounce back boundary condition expressed in Eq. (24).

Next, the boundary condition corresponding to the prescribed velocity boundary condition in Eq. (25) is derived as

$$\begin{aligned} \Theta_{\mathrm{V}} &= \int_I \int_{\Gamma_{\mathrm{V}}} \frac{1}{3} \sum_{i=1}^{9} \delta f_i \mathrm{d}\Gamma \mathrm{d}t + \int_I \int_{\Gamma_{\mathrm{V}}} \sum_{i=1}^{9} (\boldsymbol{c}_i \cdot \boldsymbol{n}) \delta f_i^{\mathrm{b}} \tilde{f}_i \mathrm{d}\Gamma \mathrm{d}t \\ &= \int_I \int_{\Gamma_{\mathrm{V}}} \left( \frac{1}{3} \sum_{i=1}^{9} \delta f_i - \tilde{f}_3 \delta f_3 + \tilde{f}_5 \delta f_5 - \tilde{f}_6 \delta f_6 - \tilde{f}_7 \delta f_7 + \tilde{f}_8 \delta f_8 + \tilde{f}_9 \delta f_9 \right) \mathrm{d}\Gamma \mathrm{d}t, \end{aligned} \tag{B.3}$$

where, based on Eq. (25), $\delta f_3$, $\delta f_6$, and $\delta f_7$ are represented as follows:

$$\begin{cases} \delta f_3 = \delta f_5 + \frac{2}{3}\rho' v_0 \\ \delta f_6 = \delta f_8 + \frac{1}{6}\rho' v_0 - \frac{1}{2}(\delta f_2 - \delta f_4) \\ \delta f_7 = \delta f_9 + \frac{1}{6}\rho' v_0 + \frac{1}{2}(\delta f_2 - \delta f_4), \end{cases} \tag{B.4}$$

where

$$\rho' = \frac{\delta f_1 + \delta f_2 + \delta f_4 + 2(\delta f_5 + \delta f_8 + \delta f_9)}{1 - v_0}. \tag{B.5}$$

Equation (B.3) can be rewritten as

$$\begin{aligned}\Theta_{\mathrm{V}} = \int_I \int_{\Gamma_{\mathrm{V}}} \Bigg\{ & \frac{1}{3}\sum_{i=1}^{9} \delta f_i - \tilde{f}_3 \left( \delta f_5 + \frac{2}{3}\rho' v_0 \right) + \tilde{f}_5 \delta f_5 \\ & - \tilde{f}_6 \left( \delta f_8 + \frac{1}{6}\rho' v_0 - \frac{1}{2}(\delta f_2 - \delta f_4) \right) \\ & - \tilde{f}_7 \left( \delta f_9 + \frac{1}{6}\rho' v_0 + \frac{1}{2}(\delta f_2 - \delta f_4) \right) + \tilde{f}_8 \delta f_8 + \tilde{f}_9 \delta f_9 \Bigg\} \mathrm{d}\Gamma \mathrm{d}t, \end{aligned} \tag{B.6}$$

in which we assume that $\delta f_{1,2,4} = 0$ is naturally satisfied when the velocity at $\Gamma_{\mathrm{V}}$ is orthogonal to this boundary. Thus, we obtain the following equation,

$$\begin{aligned}\Theta_{\mathrm{V}} = \int_I \int_{\Gamma_{\mathrm{V}}} \Bigg\{ & \delta f_5 \left( \frac{2}{3(1-v_0)} - \tilde{f}_3 + \tilde{f}_5 - \frac{v_0}{1-v_0} \left( \frac{4}{3}\tilde{f}_3 + \frac{1}{3}\tilde{f}_6 + \frac{1}{3}\tilde{f}_7 \right) \right) \\ & + \delta f_8 \left( \frac{2}{3(1-v_0)} - \tilde{f}_6 + \tilde{f}_8 - \frac{v_0}{1-v_0} \left( \frac{4}{3}\tilde{f}_3 + \frac{1}{3}\tilde{f}_6 + \frac{1}{3}\tilde{f}_7 \right) \right) \\ & + \delta f_9 \left( \frac{2}{3(1-v_0)} - \tilde{f}_7 + \tilde{f}_9 - \frac{v_0}{1-v_0} \left( \frac{4}{3}\tilde{f}_3 + \frac{1}{3}\tilde{f}_6 + \frac{1}{3}\tilde{f}_7 \right) \right) \Bigg\} \mathrm{d}\Gamma \mathrm{d}t. \end{aligned} \tag{B.7}$$

As a result, the boundary condition on $\Gamma_{\mathrm{V}}$ for the adjoint equation is defined as follows:

$$\left.\begin{aligned} \tilde{f}_5 &= -\tfrac{2}{3(1-v_0)} + \tilde{f}_3 + \tfrac{v_0}{3(1-v_0)} \left( 4\tilde{f}_3 + \tilde{f}_6 + \tilde{f}_7 \right) \\ \tilde{f}_8 &= -\tfrac{2}{3(1-v_0)} + \tilde{f}_6 + \tfrac{v_0}{3(1-v_0)} \left( 4\tilde{f}_3 + \tilde{f}_6 + \tilde{f}_7 \right) \\ \tilde{f}_9 &= -\tfrac{2}{3(1-v_0)} + \tilde{f}_7 + \tfrac{v_0}{3(1-v_0)} \left( 4\tilde{f}_3 + \tilde{f}_6 + \tilde{f}_7 \right) \end{aligned}\right\} \text{ on } \Gamma_{\mathrm{V}}. \tag{B.8}$$

The boundary condition corresponding to the prescribed pressure boundary condition expressed in Eq. (26) is derived as

$$\begin{aligned}\Theta_{\mathrm{P}} &= -\int_I \int_{\Gamma_{\mathrm{P}}} \frac{1}{3}\sum_{i=1}^{9} \delta f_i \mathrm{d}\Gamma \mathrm{d}t + \int_I \int_{\Gamma_{\mathrm{P}}} \sum_{i=1}^{9} (\boldsymbol{c}_i \cdot \boldsymbol{n}) \delta f_i^{\mathrm{b}} \tilde{f}_i \mathrm{d}\Gamma \mathrm{d}t \\ &= \int_I \int_{\Gamma_{\mathrm{P}}} \left( -\frac{1}{3}\sum_{i=1}^{9} \delta f_i - \tilde{f}_3 \delta f_3 + \tilde{f}_5 \delta f_5 - \tilde{f}_6 \delta f_6 - \tilde{f}_7 \delta f_7 + \tilde{f}_8 \delta f_8 + \tilde{f}_9 \delta f_9 \right) \mathrm{d}\Gamma \mathrm{d}t, \end{aligned} \tag{B.9}$$

where, based on Eq. (26), $\delta f_3$, $\delta f_6$, and $\delta f_7$ are represented as

$$\begin{cases} \delta f_3 = \delta f_5 + \frac{2}{3}\rho_0 v' \\ \delta f_6 = \delta f_8 + \frac{1}{6}\rho_0 v' - \frac{1}{2}(\delta f_2 - \delta f_4) \\ \delta f_7 = \delta f_9 + \frac{1}{6}\rho_0 v' + \frac{1}{2}(\delta f_2 - \delta f_4), \end{cases} \tag{B.10}$$

where

$$v' = -\frac{\delta f_1 + \delta f_2 + \delta f_4 + 2(\delta f_5 + \delta f_8 + \delta f_9)}{\rho_0}. \tag{B.11}$$

Equation (B.9) can be rewritten as

$$\begin{aligned}\Theta_{\mathrm{P}} = \int_I \int_{\Gamma_{\mathrm{P}}} \Bigg\{ & -\frac{1}{3}\sum_{i=1}^{9} \delta f_i - \tilde{f}_3 \left( \delta f_5 + \frac{2}{3}\rho_0 v' \right) + \tilde{f}_5 \delta f_5 \\ & - \tilde{f}_6 \left( \delta f_8 + \frac{1}{6}\rho_0 v' - \frac{1}{2}(\delta f_2 - \delta f_4) \right) \\ & - \tilde{f}_7 \left( \delta f_9 + \frac{1}{6}\rho_0 v' + \frac{1}{2}(\delta f_2 - \delta f_4) \right) + \tilde{f}_8 \delta f_8 + \tilde{f}_9 \delta f_9 \Bigg\} \mathrm{d}\Gamma \mathrm{d}t, \end{aligned} \tag{B.12}$$

in which we assume that $\delta f_{1,2,4}=0$ is naturally satisfied when the velocity at $\Gamma_{\mathrm{P}}$ is orthogonal to this boundary. Thus, we obtain the following:

$$\begin{aligned}\Theta_{\mathrm{P}}=\int_I\int_{\Gamma_{\mathrm{P}}}\Bigg\{&\delta f_5\left(-\frac{1}{3}\tilde{f}_3+\frac{4}{3}\tilde{f}_3+\tilde{f}_5+\frac{1}{3}\tilde{f}_6+\frac{1}{3}\tilde{f}_7\right)\\&+\delta f_8\left(\frac{4}{3}\tilde{f}_3+\tilde{f}_8-\tilde{f}_6+\frac{1}{3}\tilde{f}_6+\frac{1}{3}\tilde{f}_7\right)\\&+\delta f_9\left(\frac{4}{3}\tilde{f}_3+\tilde{f}_9+\frac{1}{3}\tilde{f}_6-\tilde{f}_7+\frac{1}{3}\tilde{f}_7\right)\Bigg\}\mathrm{d}\Gamma\mathrm{d}t.\end{aligned}\tag{B.13}$$

Consequently, the boundary condition on $\Gamma_{\mathrm{P}}$ for the adjoint equation is defined as follows:

$$\left.\begin{aligned}\tilde{f}_5&=\tilde{f}_3-\tfrac{1}{3}\left(4\tilde{f}_3+\tilde{f}_6+\tilde{f}_7\right)\\\tilde{f}_8&=\tilde{f}_6-\tfrac{1}{3}\left(4\tilde{f}_3+\tilde{f}_6+\tilde{f}_7\right)\\\tilde{f}_9&=\tilde{f}_7-\tfrac{1}{3}\left(4\tilde{f}_3+\tilde{f}_6+\tilde{f}_7\right)\end{aligned}\right\}\ \text{on }\Gamma_{\mathrm{P}}.\tag{B.14}$$

In the pressure drop minimization problem based on the proposed method, the adjoint equation in Eq. (47) is solved using the initial condition expressed in Eq. (48), and the boundary conditions expressed in Eqs. (49)–(51). In addition, we note that boundary conditions other than those presented above can be used, including a higher accuracy method (e.g., [30,47]), in fluid flow optimization problems using the LBM.

## Appendix C. Derivation of the adjoint boundary conditions for the heat exchange maximization problem

We first consider the adjoint boundary condition for the adiabatic boundary, $\Gamma_{\mathrm{W}}\cup\Gamma_{\mathrm{P}}$. In the following, only $\Gamma_{\mathrm{P}}$ is treated, since $\Gamma_{\mathrm{W}}$ is the specific case when $\boldsymbol{u}=\boldsymbol{0}$. The adjoint boundary condition for $\Gamma_{\mathrm{P}}$ can be derived as follows:

$$\begin{aligned}\Theta_{\mathrm{A}}&=\int_I\int_{\Gamma_{\mathrm{P}}}\sum_{i=1}^{9}(\boldsymbol{c}_i\cdot\boldsymbol{n})\delta g_i^{\mathrm{b}}\tilde{g}_i\mathrm{d}\Gamma\mathrm{d}t\\&=\int_I\int_{\Gamma_{\mathrm{P}}}\left(-\tilde{g}_3\delta g_3+\tilde{g}_5\delta g_5-\tilde{g}_6\delta g_6-\tilde{g}_7\delta g_7+\tilde{g}_8\delta g_8+\tilde{g}_9\delta g_9\right)\mathrm{d}\Gamma\mathrm{d}t,\end{aligned}\tag{C.1}$$

where, based on Eq. (27), $\delta g_3$, $\delta g_6$, and $\delta g_7$ are represented as follows:

$$\begin{cases}\delta g_3=\frac{1}{9}T'(1+3v)+\frac{1}{3}Tv'\\\delta g_6=\frac{1}{36}T'(1+3v)+\frac{1}{12}Tv'\\\delta g_7=\frac{1}{36}T'(1+3v)+\frac{1}{12}Tv',\end{cases}\tag{C.2}$$

where

$$T'=\frac{6(\delta g_5+\delta g_8+\delta g_9)}{1-3v}+\frac{18(g_5+g_8+g_9)}{(1-3v)^2}v',\tag{C.3}$$

and $v'$ is given by Eq. (B.11). Equation (C.1) can be rewritten as

$$\begin{aligned}\Theta_{\mathrm{A}}=\int_I\int_{\Gamma_{\mathrm{P}}}\Bigg\{&-\tilde{g}_3\left(\frac{1}{9}T'(1+3v)+\frac{1}{3}Tv'\right)+\tilde{g}_5\delta g_5\\&-\tilde{g}_6\left(\frac{1}{36}T'(1+3v)+\frac{1}{12}Tv'\right)\\&-\tilde{g}_7\left(\frac{1}{36}T'(1+3v)+\frac{1}{12}Tv'\right)+\tilde{g}_8\delta g_8+\tilde{g}_9\delta g_9\Bigg\}\mathrm{d}\Gamma\mathrm{d}t\\=\int_I\int_{\Gamma_{\mathrm{P}}}\Bigg\{&\delta g_5\left(\frac{1+3v}{1-3v}\left(-\frac{2}{3}\tilde{g}_3-\frac{1}{6}\tilde{g}_6-\frac{1}{6}\tilde{g}_7\right)+\tilde{g}_5\right)\\&+\delta g_8\left(\frac{1+3v}{1-3v}\left(-\frac{2}{3}\tilde{g}_3-\frac{1}{6}\tilde{g}_6-\frac{1}{6}\tilde{g}_7\right)+\tilde{g}_8\right)\end{aligned}$$

$$+\delta g_9\left(\frac{1+3v}{1-3v}\left(-\frac{2}{3}\tilde{g}_3-\frac{1}{6}\tilde{g}_6-\frac{1}{6}\tilde{g}_7\right)+\tilde{g}_9\right)$$
$$+v'\left(\frac{T(1+3v)}{1-3v}\left(-\frac{2}{3}\tilde{g}_3-\frac{1}{6}\tilde{g}_6-\frac{1}{6}\tilde{g}_7\right)\right)\Bigg\}\mathrm{d}\Gamma\mathrm{d}t. \tag{C.4}$$

Consequently, the boundary condition on $\Gamma_\mathrm{P}$ for the adjoint equation is defined as

$$\left.\begin{aligned}\tilde{g}_5&=\tfrac{1+3v}{6(1-3v)}(4\tilde{g}_3+\tilde{g}_6+\tilde{g}_7)\\ \tilde{g}_8&=\tfrac{1+3v}{6(1-3v)}(4\tilde{g}_3+\tilde{g}_6+\tilde{g}_7)\\ \tilde{g}_9&=\tfrac{1+3v}{6(1-3v)}(4\tilde{g}_3+\tilde{g}_6+\tilde{g}_7)\end{aligned}\right\}\ \text{on } \Gamma_\mathrm{P}. \tag{C.5}$$

Due to $v'\neq 0$ on $\Gamma_\mathrm{P}$, the adjoint boundary condition for $\tilde{f}_i$ is defined as

$$\left.\begin{aligned}\tilde{f}_5&=\tilde{f}_3-\tfrac{1}{3}\left(4\tilde{f}_3+\tilde{f}_6+\tilde{f}_7\right)-\tfrac{12T(1+3v)}{\rho_0(1-3v)}(4\tilde{g}_3+\tilde{g}_6+\tilde{g}_7)\\ \tilde{f}_8&=\tilde{f}_6-\tfrac{1}{3}\left(4\tilde{f}_3+\tilde{f}_6+\tilde{f}_7\right)-\tfrac{12T(1+3v)}{\rho_0(1-3v)}(4\tilde{g}_3+\tilde{g}_6+\tilde{g}_7)\\ \tilde{f}_9&=\tilde{f}_7-\tfrac{1}{3}\left(4\tilde{f}_3+\tilde{f}_6+\tilde{f}_7\right)-\tfrac{12T(1+3v)}{\rho_0(1-3v)}(4\tilde{g}_3+\tilde{g}_6+\tilde{g}_7)\end{aligned}\right\}\ \text{on } \Gamma_\mathrm{P}. \tag{C.6}$$

Next, the boundary condition corresponding to the prescribed temperature condition, expressed in Eq. (28) is derived as

$$\begin{aligned}\Theta_\mathrm{T}&=\int_I\int_{\Gamma_\mathrm{V}}\sum_{i=1}^{9}(\boldsymbol{c}_i\cdot\boldsymbol{n})\delta g_i^\mathrm{b}\tilde{g}_i\mathrm{d}\Gamma\mathrm{d}t\\ &=\int_I\int_{\Gamma_\mathrm{V}}\left(-\tilde{g}_3\delta g_3+\tilde{g}_5\delta g_5-\tilde{g}_6\delta g_6-\tilde{g}_7\delta g_7+\tilde{g}_8\delta g_8+\tilde{g}_9\delta g_9\right)\mathrm{d}\Gamma\mathrm{d}t,\end{aligned} \tag{C.7}$$

where, based on Eq. (28), $\delta g_3$, $\delta g_6$, and $\delta g_7$ are represented as follows:

$$\begin{cases}\delta g_3=\frac{1}{9}T'(1+3v)\\ \delta g_6=\frac{1}{36}T'(1+3v)\\ \delta g_7=\frac{1}{36}T'(1+3v),\end{cases} \tag{C.8}$$

where

$$T'=-\frac{6(\delta g_1+\delta g_2+\delta g_4+\delta g_5+\delta g_8+\delta g_9)}{1+3v}. \tag{C.9}$$

Thus, Eq. (C.7) can be rewritten as

$$\begin{aligned}\Theta_\mathrm{T}=&\int_I\int_{\Gamma_\mathrm{V}}\Bigg\{-\tilde{g}_3\left(\frac{1}{9}T'(1+3v)\right)+\tilde{g}_5\delta g_5-\tilde{g}_6\left(\frac{1}{36}T'(1+3v)\right)\\ &-\tilde{g}_7\left(\frac{1}{36}T'(1+3v)\right)+\tilde{g}_8\delta g_8+\tilde{g}_9\delta g_9\Bigg\}\mathrm{d}\Gamma\mathrm{d}t\\ =&\int_I\int_{\Gamma_\mathrm{V}}\Bigg\{\delta g_5\left(\frac{2}{3}\tilde{g}_3+\frac{1}{6}\tilde{g}_6+\frac{1}{6}\tilde{g}_7+\tilde{g}_5\right)+\delta g_8\left(\frac{2}{3}\tilde{g}_3+\frac{1}{6}\tilde{g}_6+\frac{1}{6}\tilde{g}_7+\tilde{g}_8\right)\\ &+\delta g_9\left(\frac{2}{3}\tilde{g}_3+\frac{1}{6}\tilde{g}_6+\frac{1}{6}\tilde{g}_7+\tilde{g}_9\right)\Bigg\}\mathrm{d}\Gamma\mathrm{d}t.\end{aligned} \tag{C.10}$$

Consequently, the boundary condition on $\Gamma_\mathrm{V}$ for the adjoint equation is defined as

$$\left.\begin{aligned}\tilde{g}_5&=-\tfrac{1}{6}(4\tilde{g}_3+\tilde{g}_6+\tilde{g}_7)\\ \tilde{g}_8&=-\tfrac{1}{6}(4\tilde{g}_3+\tilde{g}_6+\tilde{g}_7)\\ \tilde{g}_9&=-\tfrac{1}{6}(4\tilde{g}_3+\tilde{g}_6+\tilde{g}_7)\end{aligned}\right\}\ \text{on } \Gamma_\mathrm{V}. \tag{C.11}$$

## References


[1] O. Pironneau, On optimum profiles in Stokes flow, J. Fluid Mech. 59 (1) (1973) 117–128.
[2] B. Mohammadi, O. Pironneau, Applied Shape Optimization for Fluid, Oxford University Press, Oxford, 2001.
[3] M.P. Bendsøe, N. Kikuchi, Generating optimal topologies in structural design using a homogenization method, Comput. Methods Appl. Mech. Eng. 71 (2) (1988) 197–224.
[4] M.P. Bendsøe, O. Sigmund, Topology Optimization: Theory, Methods and Applications, Springer, New York, 2003.
[5] O. Sigmund, K. Maute, Topology optimization approaches, Struct. Multidiscip. Optim. 48 (6) (2013) 1031–1055.
[6] T. Borrvall, J. Petersson, Topology optimization of fluids in Stokes flow, Int. J. Numer. Methods Fluids 41 (1) (2003) 77–107.
[7] A. Gersborg-Hansen, O. Sigmund, R.B. Haber, Topology optimization of channel flow problems, Struct. Multidiscip. Optim. 30 (3) (2005) 181–192.
[8] Y. Deng, Z. Liu, P. Zhang, Y. Liu, Y. Wu, Topology optimization of unsteady incompressible Navier–Stokes flows, J. Comput. Phys. 230 (17) (2011) 6688–6708.
[9] S. Kreissl, K. Maute, Levelset based fluid topology optimization using the extended finite element method, Struct. Multidiscip. Optim. 46 (3) (2012) 311–326.
[10] A. Evgrafov, Topology optimization of slightly compressible fluids, Z. Angew. Math. Mech. 86 (1) (2006) 46–62.
[11] F. Brezzi, M. Fortin, Mixed and Hybrid Finite Element Methods, Springer-Verlag, Berlin, 1991.
[12] G.R. McNamura, G. Zanetti, Use of the Boltzmann equation to simulate lattice-gas automata, Phys. Rev. Lett. 61 (20) (1988) 2332–2335.
[13] F. Higuera, S. Succi, R. Benzi, Lattice gas dynamics with enhanced collisions, Europhys. Lett. 9 (4) (1989) 345–349.
[14] S. Chen, G.D. Doolen, Lattice Boltzmann method for fluid flows, Annu. Rev. Fluid Mech. 30 (1) (1998) 329–364.
[15] S. Succi, Lattice Boltzmann Equation for Fluid Dynamics and Beyond, Oxford University Press, New York, 2001.
[16] G. Pingen, A. Evgrafov, K. Maute, Topology optimization of flow domains using the lattice Boltzmann method, Struct. Multidiscip. Optim. 34 (6) (2007) 507–524.
[17] D. Makhija, G. Pingen, R. Yang, K. Maute, Topology optimization of multi-component flows using a multi-relaxation time lattice Boltzmann method, Comput. Fluids 67 (2012) 104–114.
[18] F. Higuera, J. Jimenez, Boltzmann approach to lattice gas simulations, Europhys. Lett. 9 (7) (1989) 663–668.
[19] S. Kreissl, G. Pingen, A. Evgrafov, K. Maute, Topology optimization of flexible micro-fluidic devices, Struct. Multidiscip. Optim. 42 (4) (2010) 495–516.
[20] G. Pingen, A. Evgrafov, K. Maute, A parallel Schur complement solver for the solution of the adjoint steady-state lattice Boltzmann equations: application to design optimisation, Int. J. Comput. Fluid Dyn. 22 (7) (2008) 457–464.
[21] M. Tekitek, M. Bouzidi, F. Dubois, P. Lallemand, Adjoint lattice Boltzmann equation for parameter identification, Comput. Fluids 35 (8) (2006) 805–813.
[22] M.J. Krause, Fluid flow simulation and optimisation with lattice Boltzmann methods on high performance computers: application to the human respiratory system, Karlsruhe Institute of Technology, KIT, 2010.
[23] M.J. Krause, G. Thäter, V. Heuveline, Adjoint-based fluid flow control and optimisation with lattice Boltzmann methods, Comput. Math. Appl. 65 (6) (2013) 945–960.
[24] P.L. Bhatnagar, E.P. Gross, M. Krook, A model for collision processes in gases. I. Small amplitude processes in charged and neutral one-component systems, Phys. Rev. 94 (3) (1954) 511–525.
[25] K. Yaji, T. Yamada, M. Yoshino, T. Matsumoto, K. Izui, S. Nishiwaki, Topology optimization using the lattice Boltzmann method incorporating level set boundary expressions, J. Comput. Phys. 274 (2014) 158–181.
[26] G. Liu, M. Geier, Z. Liu, M. Krafczyk, T. Chen, Discrete adjoint sensitivity analysis for fluid flow topology optimization based on the generalized lattice Boltzmann method, Comput. Math. Appl. 68 (10) (2014) 1374–1392.
[27] K. Yonekura, Y. Kanno, A flow topology optimization method for steady state flow using transient information of flow field solved by lattice Boltzmann method, Struct. Multidiscip. Optim. 51 (1) (2014) 159–172.
[28] Q. Zou, X. He, On pressure and velocity boundary conditions for the lattice Boltzmann BGK model, Phys. Fluids 9 (6) (1997) 1591–1598.
[29] T. Inamuro, M. Yoshino, F. Ogino, A non-slip boundary condition for lattice Boltzmann simulations, Phys. Fluids 7 (12) (1995) 2928–2930, Erratum: Phys. Fluids 8 (4) (1996) 1124.
[30] R.S. Maier, R.S. Bernard, D.W. Grunau, Boundary conditions for the lattice Boltzmann method, Phys. Fluids 8 (7) (1996) 1788–1801.
[31] R. Mei, W. Shyy, D. Yu, L.-S. Luo, Lattice Boltzmann method for 3-D flows with curved boundary, J. Comput. Phys. 161 (2) (2000) 680–699.
[32] T. Inamuro, M. Yoshino, H. Inoue, R. Mizuno, F. Ogino, A lattice Boltzmann method for a binary miscible fluid mixture and its application to a heat-transfer problem, J. Comput. Phys. 179 (1) (2002) 201–215.
[33] Y. Sone, Asymptotic theory of flow of rarefied gas over a smooth boundary II, in: D. Dini (Ed.), Rarefied Gas Dynamics, Editrice Tecnico Scientifica, Pisa, 1971, pp. 737–749.
[34] M. Yoshino, T. Inamuro, Lattice Boltzmann simulations for flow and heat/mass transfer problems in a three-dimensional porous structure, Int. J. Numer. Methods Fluids 43 (2) (2003) 183–198.
[35] T. Matsumori, T. Kondoh, A. Kawamoto, T. Nomura, Topology optimization for fluid–thermal interaction problems under constant input power, Struct. Multidiscip. Optim. 47 (4) (2013) 571–581.
[36] K. Yaji, T. Yamada, S. Kubo, K. Izui, S. Nishiwaki, A topology optimization method for a coupled thermal-fluid problem using level set boundary expressions, Int. J. Heat Mass Transf. 81 (2015) 878–888.
[37] C.S. Andreasen, A.R. Gersborg, O. Sigmund, Topology optimization of microfluidic mixers, Int. J. Numer. Methods Fluids 61 (5) (2009) 498–513.
[38] D. Makhija, K. Maute, Level set topology optimization of scalar transport problems, Struct. Multidiscip. Optim. 51 (2) (2015) 267–285.
[39] E. Vergnault, P. Sagaut, An adjoint-based lattice Boltzmann method for noise control problems, J. Comput. Phys. 276 (2014) 39–61.
[40] K. Ito, K. Kunisch, Lagrange Multiplier Approach to Variational Problems and Applications, vol. 15, SIAM, 2008.
[41] K. Svanberg, The method of moving asymptotes—a new method for structural optimization, Int. J. Numer. Methods Eng. 24 (2) (1987) 359–373.
[42] J.K. Guest, J. Prévost, T. Belytschko, Achieving minimum length scale in topology optimization using nodal design variables and projection functions, Int. J. Numer. Methods Eng. 61 (2) (2004) 238–254.
[43] J.K. Guest, J.H. Prévost, Topology optimization of creeping fluid flows using a Darcy–Stokes finite element, Int. J. Numer. Methods Eng. 66 (3) (2006) 461–484.
[44] V.J. Challis, J.K. Guest, Level set topology optimization of fluids in Stokes flow, Int. J. Numer. Methods Eng. 79 (10) (2009) 1284–1308.
[45] L.H. Olesen, F. Okkels, H. Bruus, A high-level programming-language implementation of topology optimization applied to steady-state Navier–Stokes flow, Int. J. Numer. Methods Eng. 65 (7) (2006) 975–1001.
[46] S. Lin, L. Zhao, J.K. Guest, T.P. Weihs, Z. Liu, Topology optimization of fixed-geometry fluid diodes, J. Mech. Des. 137 (8) (2015) 081402.
[47] S. Chen, D. Martinez, R. Mei, On boundary conditions in lattice Boltzmann methods, Phys. Fluids 8 (9) (1996) 2527–2536.